Molecular Imaging of Cardiovascular Inflammation

Neil MacRitchie[1,2], Jonathan Noonan[3], Tomasz J. Guzik[2,4], Pasquale Maffia[1,2,5]

[1]*Centre for Immunobiology, Institute of Infection, Immunity and Inflammation, College of Medical, Veterinary and Life Sciences, University of Glasgow, Glasgow, United Kingdom*

[2]*Institute of Cardiovascular and Medical Sciences, College of Medical, Veterinary and Life Sciences, University of Glasgow, Glasgow, United Kingdom*

[3]*Baker Heart and Diabetes Institute, Melbourne, Australia*

[4]*Department of Internal Medicine, Jagiellonian University, Collegium Medicum, Kraków, Poland*

[5]*Department of Pharmacy, University of Naples Federico II, Naples, Italy*

Correspondence Pasquale Maffia, Institute of Infection, Immunity and Inflammation, College of Medical, Veterinary and Life Sciences, University of Glasgow, Sir Graeme Davies Building, 120 University Place, Glasgow G12 8TA, Glasgow, United Kingdom. E-mail: Pasquale.Maffia@glasgow.ac.uk and Neil MacRitchie Neil.MacRitchie@glasgow.ac.uk

Abbreviations

^{18}F- fluorodeoxyglucose (^{18}F-FDG); abdominal aortic aneurysm (AAA); adverse cardiac events (ACEs); Canakinumab Anti-inflammatory Thrombosis Outcome Study (CANTOS); cardiovascular disease (CVD); contrast to noise ratio (CNR); computed tomography (CT); computed tomography angiography (CTA); contrast-enhanced ultrasound (CEUS); electrocardiogram (ECG); fat attenuation index (FAI); fat radiomic profile (FRP); fluorescence emission computed tomography (FLECT); gadolinium (Gd^{3+}); gold NP core (AuNP); indocyanine green (ICG); intravascular ultrasound (IVUS); kinase insert domain receptor (KDR); late gadolinium enhancement (LGE); left anterior descending coronary artery (LAD); left ventricle (LV); major adverse cardiac events (MACE); magnetic particle imaging (MPI); magnetic resonance imaging (MRI); multispectral optoacoustic tomographic (MSOT); nanoparticles (NPs); napkin-ring sign (NRS); natriuretic peptide receptor C (NPRC); Near-Infrared Fluorescence (NIRF); percutaneous coronary intervention (PCI); perfluorocarbons (PFCs); perivascular adipose tissue (PVAT); photoacoustic imaging (PAI); polyethylene

glycol (PEG); positron emitted tomography (PET); somatostatin receptors (SSTRs); standardized uptake values (SUV); super-paramagnetic iron oxide particles (SPIOs); surface-enhanced Raman spectroscopy (SERS); thin cap fibroatheroma (TCFA); transient ischaemic attack (TIA); translocator protein (TSPO); ultrasound (US).

Abstract

Cardiovascular diseases (CVD), including atherosclerosis, are chronic inflammatory diseases characterised by a complex and evolving tissue micro-environment. Molecular heterogeneity of inflammatory responses translates into clinical outcomes. However, current medical imaging modalities are unable to reveal the cellular and molecular events at a level of detail that would allow more accurate and timely diagnosis and treatment. This is an inherent limitation of the current imaging tools which are restricted to anatomical or functional data. Molecular imaging – the visualization and quantification of molecules in the body – is already established in the clinic in the form of Positron Emitted Tomography (PET), yet the use of PET in CVD is limited. In this visual review, we will guide you through the current state of molecular imaging research, assessing the respective strengths and weaknesses of molecular imaging modalities, including those already being used in the clinic such as PET and magnetic resonance imaging (MRI) and emerging technologies at pre-clinical stage, such as photoacoustic imaging. We discuss the basic principles of each technology and provide key examples of their application in imaging inflammation in CVD and the added value into the diagnostic decision-making process. Finally, we discuss barriers for rapid successful clinical translation of these novel diagnostic modalities.

Keywords

Atherosclerosis; computed tomography (CT); heart; inflammation; magnetic resonance imaging (MRI); molecular imaging; photoacoustic imaging (PAI); positron emission tomography (PET); surface-enhanced Raman spectroscopy (SERS).

Authors Contributions

All authors listed, have made substantial, direct and intellectual contribution to the work, and approved it for publication.

Molecular Imaging

Introduction

Molecular imaging is a field of imaging that focuses on imaging molecules within living organisms. These can be endogenous biomolecules or exogenous imaging agents, particularly in the context of high affinity pharmacological ligands or ligand-targeted nanomaterials. Imaging at the molecular level allows integration of biological processes at an unprecedented level of detail which could translate to significantly enhanced clinical care, including earlier and more accurate diagnosis, more effective tailoring of treatments based on a patient's disease 'signature' (personalized medicine) and greater information for narrowing the search for effective pharmaceuticals. Molecular imaging requires sophisticated imaging tools (or modalities) capable of detecting molecular changes that define disease states and allow for their more accurate than at present grading and staging (MacRitchie et al., 2017; MacRitchie et al., 2020a).

The need for earlier and improved diagnosis of cardiovascular disease

In cardiovascular disease (CVD), correct diagnosis is frequently delayed, leading to increased mortality, a greater number of diagnostic investigations and raised overall disease burden. Clinical imaging modalities can offer good specificity but low sensitivity in predicting future major cardiovascular events. Diagnostic techniques are often invasive requiring coronary catheterisation and overall,

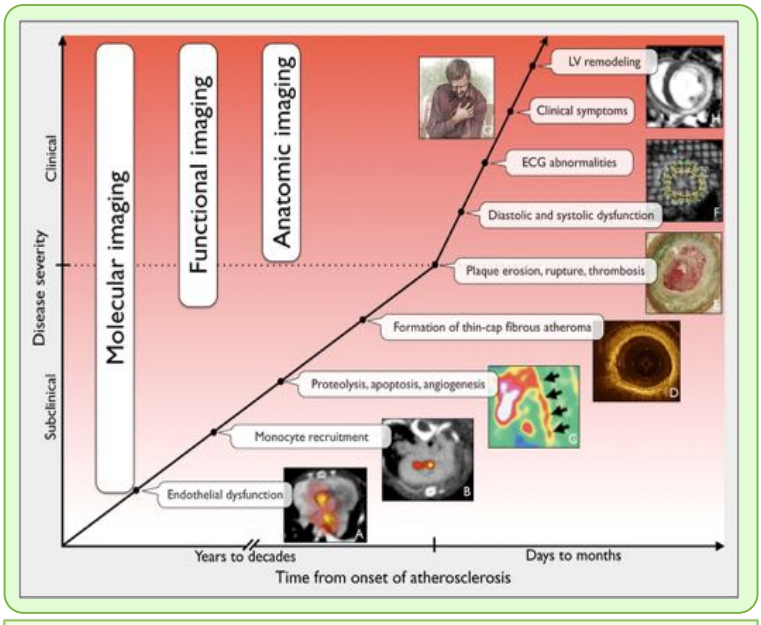

Figure 1. Early and accurate diagnosis of CVD requires molecular imaging. Reproduced from Majmudar and Nahrendorf 2012. Copyright of the Society of Nuclear Medicine and Molecular Imaging (SNMMI).

clinical imaging technologies offer only anatomical or functional level imaging. Quite importantly, as illustrated in Figure 1, most diagnostic imaging is also employed only after the patient has advanced disease. In the case of atherosclerosis, immune-inflammatory responses play crucial roles in all the stages of the pathology (Welsh et al., 2017; Ridker et al., 2017); however, current technologies cannot provide the detailed information on the nature of the plaque and the level of vascular inflammation needed to accurately predict future outcomes. To acquire such a level of detailed diagnostic data, we require molecular imaging tools that can interrogate the molecular changes in the vessel wall and plaque, such as the inflammatory status, which can be used in the asymptomatic years to characterise plaque risk in a non-invasive way, allowing prompt diagnosis and therapeutic intervention.

Molecular Imaging Modalities

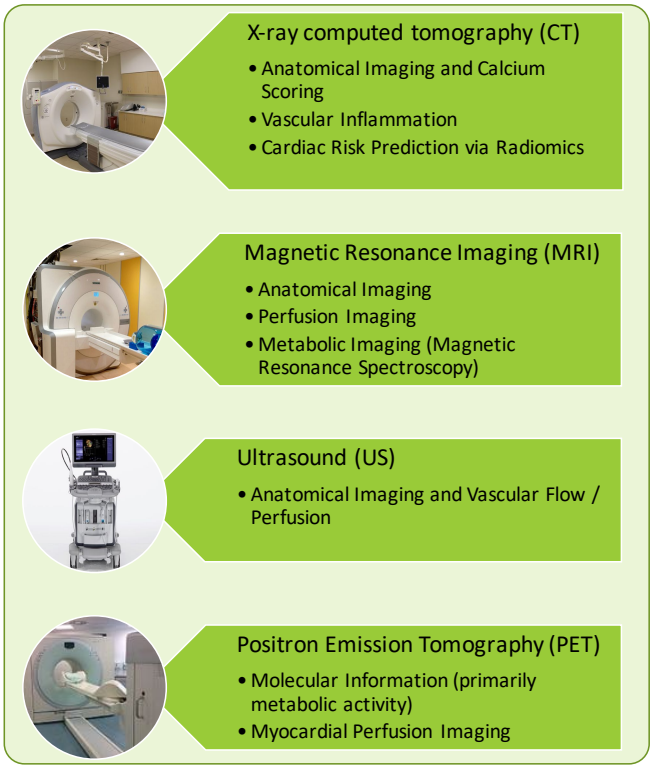

Figure 2. Medical imaging techniques commonly performed and their common uses. All photos licenced under CC-BY-SA.

A wide variety of imaging modalities are used in the investigation of cardiovascular abnormalities coupled with other tests such as cardiac stress testing, electrocardiogram (ECG) and blood biochemistry. Thus, imaging results are an important part of the diagnostic work up. Techniques that are commonly performed and their common uses are shown in Figure 2.

While only PET stands as a true molecular imaging modality within the clinic, it has significant limitations that preclude its use in all but a small number of cardiovascular disorders (discussed in the PET section). The other imaging techniques are currently employed to give anatomic or functional information (e.g. perfusion or morphological changes in cardiovascular tissue). Figure 3 illustrates the various properties that an ideal molecular imaging modality should possess. To summarize, it should possess high sensitivity (to detect low level imaging tracers or endogenous molecules) and spatial resolution

(to allow molecular mapping of inflammatory sites), fast imaging times (to minimise cost and motion artefacts and maximise patient comfort), be able to image structures at depth within the body (unless utilized solely as an invasive catheter instrument), be quantifiable and reproducible (to allow stratification and accurate monitoring of disease status across patients), have low economic burden and have the ability to assess multiple targets in a single scan, known as multiplexing. The more disease markers a clinician can image in a single scan, then the more diagnostic information is obtained, thus improving diagnostic accuracy. In reality, no current technology possesses all of these attributes at the desired level hence why hybrid technologies such as PET-CT or PET-MRI were created which can combine their respective strengths.

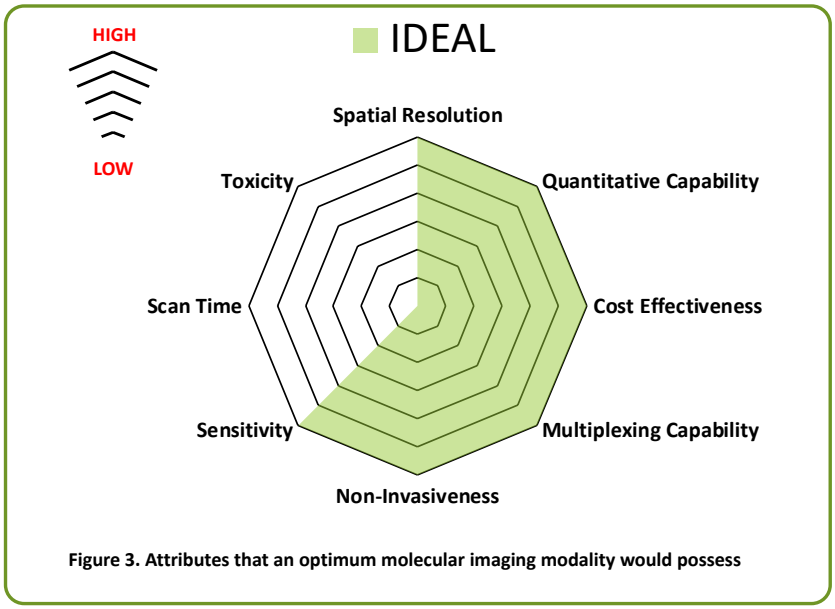

Figure 3. Attributes that an optimum molecular imaging modality would possess

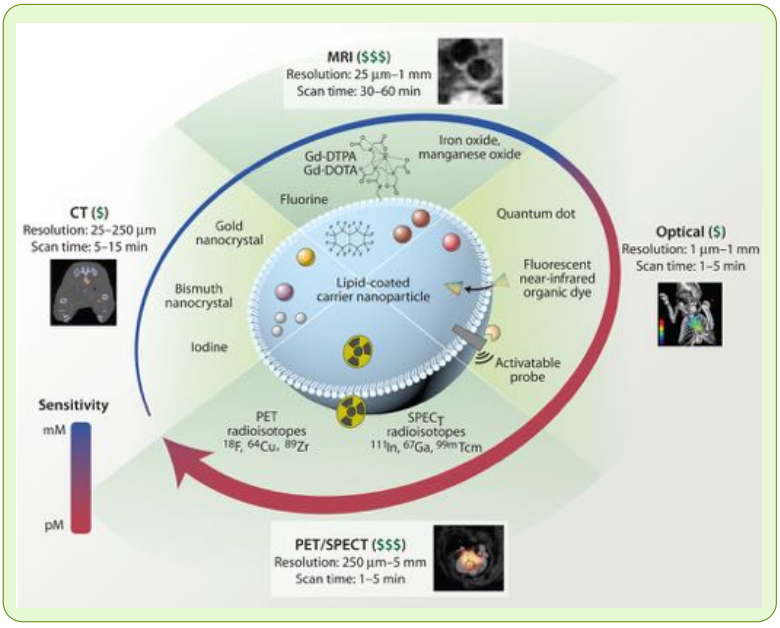

Figure 4. Properties and tracers used in selected currently available imaging modalities. The relative costs, sensitivity, scan time range, and resolution range are indicated. Sensitivity and spatial resolution often show an inverse relationship which limits potential for detailed molecular imaging at a cellular level. Each modality relies on a unique set of imaging agents (common examples shown) that may take the form of small molecules or nanoparticle (NP) sized agents of variable compositions to match the respective detection method. Reproduced from Mulder et al., 2014, Science Translational Medicine, 6(239), 239sr1. Reprinted with permission from AAAS.

It is often noticeable within clinical medical imaging technologies that an effective strength is often counter balanced by an equally prominent weakness. This is demonstrated in Figure 4. Here, we can see that there is frequently an inverse relationship between sensitivity and spatial resolution. For example, nuclear imaging

displays excellent sensitivity (down to the picomolar range) but with a spatial resolution of several mms clinically. Conversely, CT can resolve images an order of magnitude greater but requires millimolar level of contrast agent (Nazir and Nicol 2019).

Most clinical imaging modalities utilise small molecules as imaging agents such as radionucleotides in PET or gadolinium chelates in MRI. However, larger nano and micron sized particles are also employed such as iron oxide-based agents in MRI and microbubbles in contrast-enhanced ultrasound (CEUS). For molecular imaging, nanoparticles (NPs) offer many advantages over small molecules and can be tuned to desired specifications such as circulating residence times, multi-ligand targeting and can also be engineered to be detectable by more than one modality. While few nano and micron sized particles are clinically approved, pre-clinically there is a drive towards the utilisation of nanomaterials, and these may become key imaging agents in the molecular imaging scene in the years ahead. Indeed, some emerging technologies such as magnetic particle imaging (MPI) and surface-enhanced Raman spectroscopy (SERS) have a fundamental requirement for NPs to generate a signal.

Computed Tomography (CT)

Within the clinic, the low sensitivity of CT has limited its usefulness as a molecular imaging tool although its use for risk stratification based on calcium scoring is commonly applied for detecting advanced coronary and carotid plaques. Pre-clinical advancements in detecting multiples disease features have arisen from the use of spectral-CT (the ability to detect different molecules based on distinct X-ray absorption profiles). Initial experiments performed on isolated human plaques demonstrated that spectral-CT could differentiate plaque components including lipids, water and calcium, albeit with high ionising radiation exposure (Zainon et al., 2012). The use of gold-based NPs in mouse models of atherosclerosis also allow imaging of macrophage accumulation (Au-HDL particles). In combination with iodine (vascular resolving) and calcium detection, both size, location and inflammatory burden can be assessed (Cormode et al., 2012). Coronary computed tomography angiography (CTA) can also identify morphological features within coronary plaques. For example, the identification of napkin-ring sign (NRS) is a strong predictor of acute coronary syndrome events (Otsuka et al., 2013).

CT imaging is also increasingly being utilised for radiomics - the extraction of quantitative data from medical images - that can improve diagnostic sensitivity while reducing user bias (Kolossváry et al., 2019). Taking NRS as an example, radiomic assessment of 30 patients with

NRS plaques versus 30 plaques that did not display evidence of NRS revealed that 916 out of 4440 radiomic parameters were significantly different between the two cohorts while none of the conventional parameters were significantly different. This emphasises the qualitative assessment of NRS by clinicians based on conventional parameters such as plaque burden, length and attenuation and indicates that unbiased quantitative radiomics has greater power for discriminating NRS from non NRS plaques (Kolossváry et al., 2017). Moreover, Kolossváry et al., 2019 demonstrated that radiomic data derived from CT scans could identify makers of plaque vulnerability as assessed by PET or invasive intravascular ultrasound (IVUS)/optical coherence tomography (OCT). Therefore, despite imaging at the anatomic level, information pertaining to inflammation and microcalcifications, as identified via ^{18}F-NaF PET, can also be derived with high accuracy via CT radiomics (Kolossváry et al., 2019).

A recent important development is the use of CT for imaging perivascular adipose tissue (PVAT) surrounding coronary arteries. PVAT has a role in vascular homeostasis and in vascular pathology where it interacts with the underlying vessel wall via bidirectional paracrine signalling (Nosalski and Guzik, 2017). Antonopoulos et al., 2017 demonstrated that in the presence of vascular inflammation, there is a reduction in adipocyte density within PVAT and a shift towards a more aqueous state. This change in ratio of lipids to water alters the attenuation of X-rays which can be detected by coronary CT and used to create a fat attenuation index (FAI). In turn, the FAI can be used to identify the presence of underlying inflammation and predict future mortality in patients who had undergone coronary CTA (Antonopoulos et al., 2017; Oikonomou et al., 2018). More recently, a radiomic signature associated with fibrosis and increased vascularity within the coronary PVAT of patients in the SCOT-HEART trial was found to independently associate with an increased risk of major adverse cardiac events (MACE) (Oikonomou et al., 2019). Patients with a high fat radiomic profile (FRP) were 10.8 times were likely to suffer a MACE within the 5 years following CCTA. This study demonstrated that FRP adds increased prognostic value to conventional CCTA derived data (Oikonomou et al., 2019). While not a molecular imaging tool in the strictest sense, CT imaging is still able to discriminate anatomical changes with a high degree of precision and thus inform

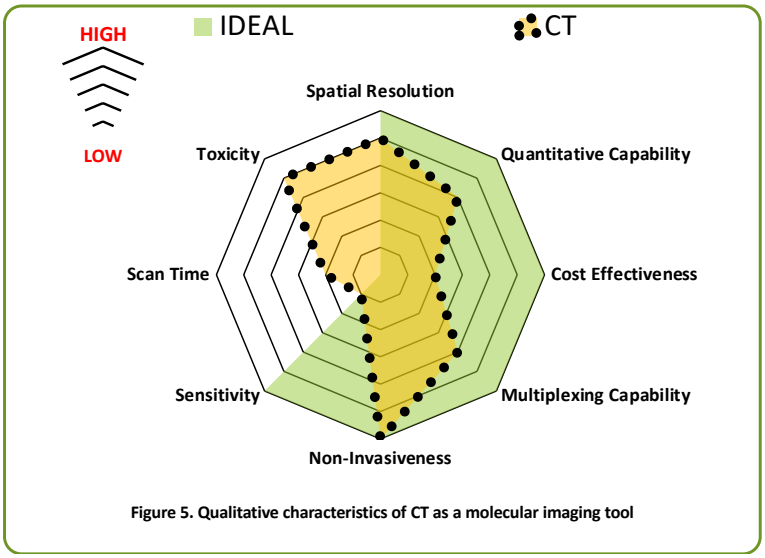

Figure 5. Qualitative characteristics of CT as a molecular imaging tool

on the underlying cellular and molecular changes that accompany vascular inflammation. Figure 5 illustrates how CT compares to our ideal molecular imaging tool from Figure 3. For a visual demonstration of perivascular fat imaging by CT, please refer to Kotanidis and Antoniades 2021 review in this special issue.

Magnetic Resonance Imaging (MRI)

MRI is a highly detailed anatomic imaging tool for monitoring changes in soft tissue structures within the body. It is also employed to provide anatomic detail for PET/SPECT. Clinically, contrast agents include paramagnetic ions, usually gadolinium (Gd^{3+}) chelates for T1 MRI or super-paramagnetic iron oxide particles (SPIOs) for T2 MRI scans. While several SPIOs have been clinically approved, many have been withdrawn due to poor performance when compared with other diagnostic tests. Molecular imaging of CVD is not a feature of current clinical MRI.

If MRI is to be implemented in this way, then higher performing biocompatible imaging agents are required.

Pre-clinical research with molecular MRI employs both T1 and T2 imaging with common targets in CVD including endothelial adhesion molecules and markers of thrombosis (MacRitchie et al., 2020a). Furthermore, while both T1/T2 MRI relies on detecting changes in ^{1}H, ^{19}F is also highly amenable to MRI imaging (Ruiz-Cabello et al., 2011), with perfluorocarbons (PFCs) (which contain a large number of ^{19}F atoms) the agents most commonly used. Since ^{19}F is present at only low concentrations in the body, ^{19}F MRI can offer great improvements in the signal to noise ratio. We now describe some pre-clinical studies that highlight the promise of these different forms of MRI in detecting inflammation in CVD.

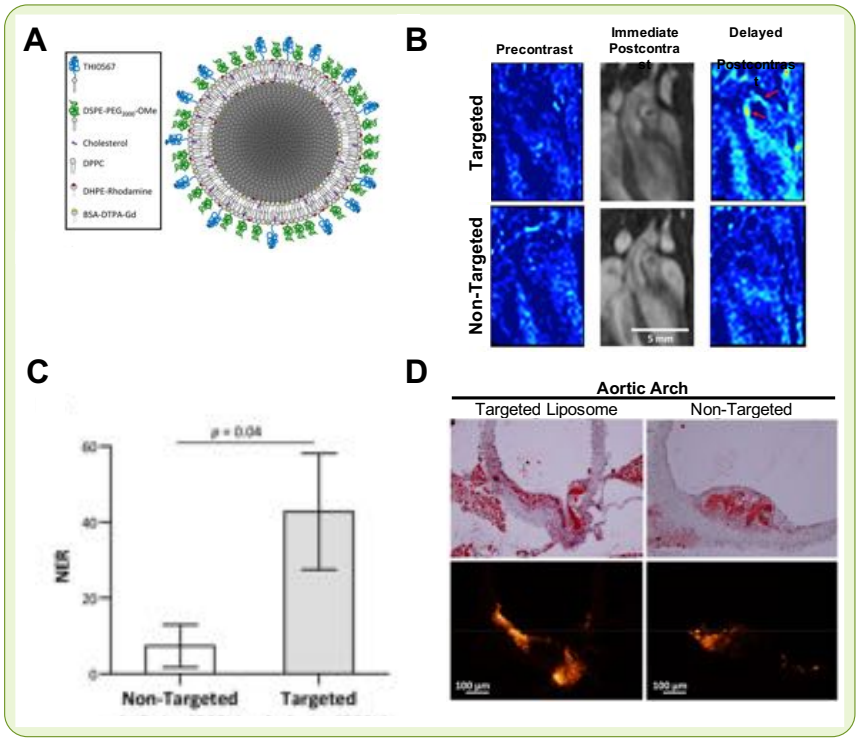

Figure 6. α4β1 – targeted liposomes for T1 imaging of atherosclerotic plaques in mice (**A**) Schematic of α4β1 targeted Gd labelled liposome. (**B**) MRI imaging, performed at 1T on apoE$^{-/-}$ mice following 10 weeks high-fat diet. Delayed post-contrast scan reveals enhanced T1 signal at locations in aorta wall where THI0567 targeted liposomes have bound. (**C**) Normalized enhancement ratios (NERs) reveal superior signal for targeted versus non-targeted liposomes. (**D**) Comparison of Oil Red O staining and rhodamine fluorescence signal from liposomes in aortic arch tissue sections. Adapted from: Woodside et al., 2018, distributed under the terms of a Creative Commons Attribution (CC BY) license (https://creativecommons.org/licenses/by/4.0/).

Figure 6 is taken from a study utilising Gd^{3+} containing liposomes targeted to α4β1, an integrin involved in leukocyte trafficking into the inflamed vasculature. It also contains rhodamine for fluorescence detection *ex vivo*. Utilising the apolipoprotein-E (apoE)$^{-/-}$ mouse model of experimental atherosclerosis and imaging at the clinical field strength of 1T, Woodside et al., 2018 demonstrated that targeted liposomes were readily detected by MRI, with the highest signal arising from the aortic arch. Liposomes are well tolerated in patients and may be a suitable vehicle for targeted molecular imaging. One advantage of a leukocyte targeted liposome such as THI0567 is added

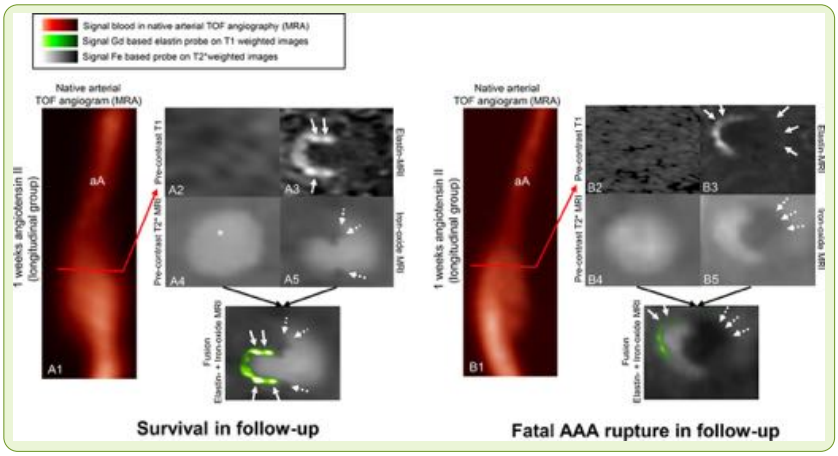

Figure 7. In vivo dual-probe MRI of inflammatory activity and ECM degradation in mice with AAA. Animals with induced AAA were injected with ferumoxytol (T2 imaging agent) and an elastic specific probe containing Gd^{3+} for T1 imaging. Uptake and accumulation of ferumoxytol appears as a signal void on T2 weighted images while uptake of the elastin targeted probe appear as a brightening on T1 weighted images. A1 shows an animal surviving AAA formation while B1 is of an animal that suffered fatal AAA rupture. When comparing these results, it can be seen that injection of ferumoxytol 1 week after angiotensin-II infusion caused a larger signal void on T2 weighted images in animals that went to suffer fatal rupture. The elastin-specific probe, also administered 1 week after ang-ii infusion, displayed a less intense signal in animals that suffered fatal rupture. Reproduced from Brangsch et al., 2019, Circulation. Cardiovascular Imaging, 12(3), e008707. Reprinted with permission from Wolters Kluwer Health, Inc. and American Heart Association, Inc.

specificity for inflammation, a feature that ^{18}F-fluorodeoxyglucose (^{18}F-FDG) imaging in PET lacks (since other metabolically active cells such as cardiomyocytes also accumulate ^{18}F-FDG leading to significant signal noise.

In an elegant study by Brangsch et al., 2019, it was demonstrated that combined T1/T2 MRI imaging utilising a dual-probe approach could effectively predict fatal abdominal aortic aneurysm (AAA) rupture via combined detection of inflammation (through SPIO uptake by macrophages) and extracellular matrix (ECM) degradation through a Gd^{3+} containing elastin-specific probe (Figures 7 and 8). Post-mortem examination of AAA sections revealed a strong correlation in macrophage accumulation

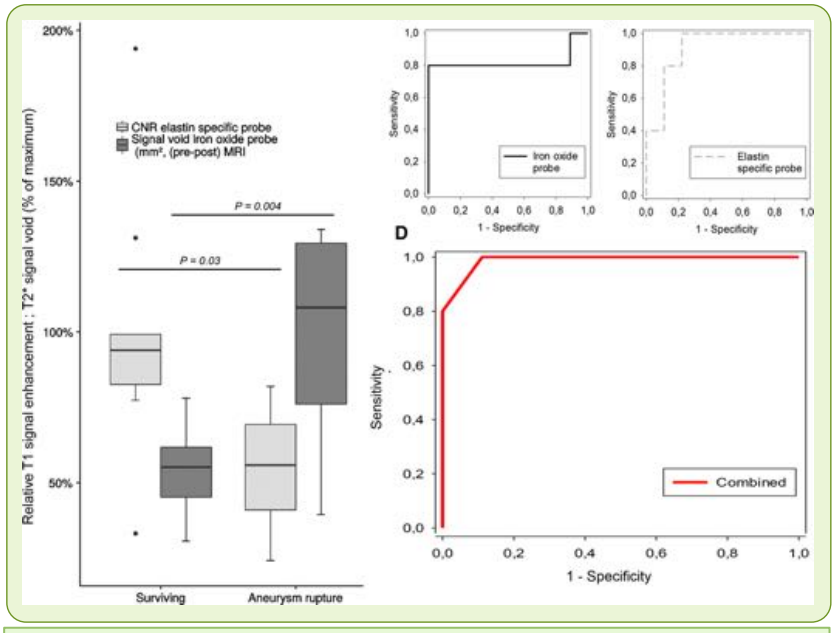

Figure 8. Diagnostic accuracy of molecular MRI of inflammatory activity and ECM degradation for the prediction of aneurysm rupture. Quantifying the imaging data shown in Figure 7 revealed that ferumoxytol caused an 85% larger signal void in T2 images in animals that suffered fatal rupture compared with surviving animals. Based on this single parameter, AAA rupture could be predicted with a sensitivity of 80% and a specificity of 89%. With respect to the elastin-specific probe, animals that died showed an 84% lower contrast to noise ratio (CNR) in T1 images compared with those that survived. Results from this probe showed that AAA rupture could be predicted with a sensitivity of 80% and a specificity of 78%. Combining the results from both T1 and T2 data resulted in a highly accurate prediction of AAA induced death with a sensitivity of 100% and a specificity of 89%. Reproduced from Brangsch et al., 2019, Circulation. Cardiovascular Imaging, 12(3), e008707. Reprinted with permission from Wolters Kluwer Health, Inc. and American Heart Association, Inc.

and elastic fibre density with *in vivo* MRI data. Therefore, this study demonstrates that simultaneous imaging of inflammatory burden and ECM degradation can be used to predict AAA severity with very high accuracy.

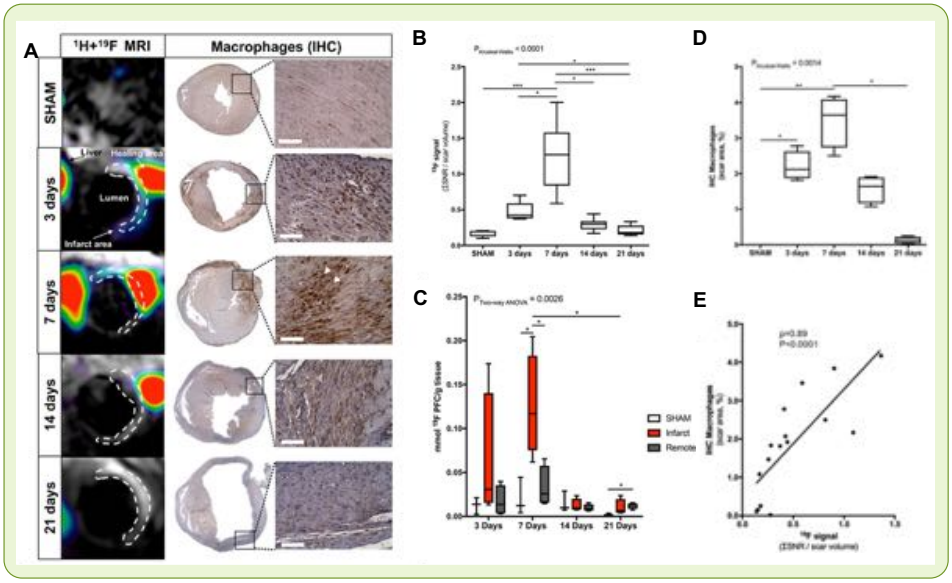

Figure 9. ^{1}H/^{19}F imaging of inflammatory burden in mice following myocardial infarction. (**A-B**) Highest intensity signal of PFC accumulation was observed on day 7. (**C**) Hearts were isolated and analysed by NMR to quantify ^{19}F uptake. (**D-E**). Macrophage density as determined by IHC showed a highly significant correlation with ^{19}F signal. Reproduced from Ramos et al., 2018, Circulation. Cardiovascular Imaging, 11(11), e007453. Reprinted with permission from Wolters Kluwer Health, Inc. and American Heart Association, Inc.

Myocardial injury very quickly results in infiltration of innate immune cells including neutrophils and macrophages to initiate tissue repair, but an extended 'hyper' inflammatory response can result in maladaptive remodelling and worse prognosis (Anzai, 2013). Part of this response also promotes excess fibrosis and non-functional scar tissue. A major component of the fibrotic tissue is secreted tropoelastin, the precursor to elastin which

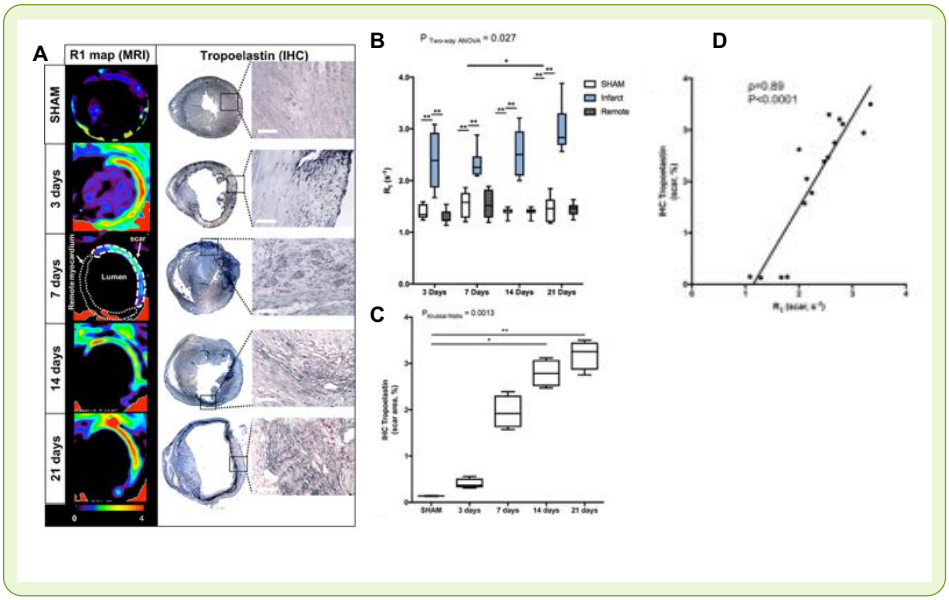

Figure 10. MRI imaging of ECM remodelling in mice after MI. (**A-C**) Relaxation rate maps show levels of Gd-ESMA uptake with uptake observed at each of the time points in infarcted areas but not in remote areas or in sham treated mice. Tropoelastin IHC revealed significantly elevated staining at 14 and 21 days in infarcted regions. (**D**) A highly significant correlation was observed between the in vivo MRI and ex vivo IHC indicating the strong specificity of this tracer for remodelled myocardium. Reproduced from Ramos et al., 2018, Circulation. Cardiovascular Imaging, 11(11), e007453. Reprinted with permission from Wolters Kluwer Health, Inc. and American Heart Association, Inc.

eventually forms elastic fibres of the scar tissue. Utilising a murine model of myocardial infarction (MI), Ramos et al., 2018 utilised dual $^{1}H/^{19}F$ MRI to simultaneously detect inflammation and fibrosis. Mice underwent left anterior descending (LAD) coronary artery occlusion to induce a model of MI or were subjected to sham surgery. Subsequently, mice were injected with a PFC suspension 48h prior to image acquisition in addition to a gadolinium containing imaging agent that binds to elastin and tropoelastin 1h prior to imaging. Imaging was performed at 3T utilising a dual $^{1}H/^{19}F$ coil (Figures 9 and 10). The same group subsequently performed additional longitudinal imaging to determine the predictive power of MRI in the MI model. They observed that the presence of inflammation at day 7 post MI was predictive of dysfunctional wound healing and the presence of scar tissue at 7 days is detrimental to cardiac remodelling (Ramos et al., 2018). Therefore, the use of this dual MRI approach may better inform on the processes of myocardial wound healing and better predict likely outcomes.

Figure 11 illustrates how MRI compares to our ideal molecular imaging tool from Figure 3. MRI has several advantages including body wide imaging, good spatial resolution (compared with nuclear imaging) and the acceptable toxicity of tracers for most patients. The major limitation of MRI is low sensitivity, particularly in comparison to PET which employs picomolar to low nanomolar levels of tracers. In contrast, MRI requires several orders of magnitude higher concentrations to generate a quantifiable signal (Sinharay and Pagel, 2016). However, this may be mitigated by PFC based agents that can deliver high concentrations of ^{19}F in a targeted manner. ^{19}F also has the advantage of being able to be used alongside T1 agents whereas T2 magnetic based probes cannot (Ramos et al., 2018). Other drawbacks of MRI include poor signal to noise and long imaging times. MRI is also relatively expensive (although considerably less expensive that PET) and costs for ^{19}F MRI will extend beyond traditional ^{1}H based systems as hardware has to be re-configured to record and analyse the ^{19}F

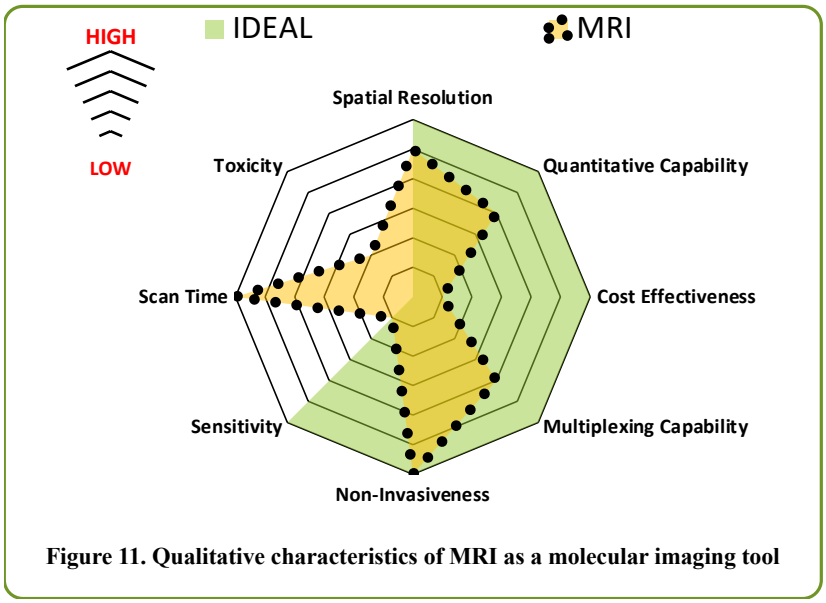

Figure 11. Qualitative characteristics of MRI as a molecular imaging tool

signal. For molecular imaging, ^{19}F MRI is a promising tool yet proof of concept for cardiovascular imaging in humans is currently lacking (Wust et al., 2019).

Positron Emission Tomography (PET)

PET is the modality that most comes to mind when the term 'molecular imaging' is used, particularly in the clinic where PET has revolutionised cancer detection and monitoring over the last 25 years. Indeed, PET today remains mostly a tool for oncologists. In the context of CVDs, PET is used clinically only for relatively uncommon conditions such as cardiac sarcoidosis, large vessel vasculitis and ischaemic cardiomyopathy; it is not part of diagnostic testing for atherosclerosis (MacAskill et al., 2019). Over 90% of PET scans use the tracer ^{18}F-FDG, with the uptake of this tracer corresponding to the metabolic activity of the cell. This not only allows detection of tumours (due to their enhanced energy utilisation) but also inflammatory cells, in particular phagocytes, that expend increased metabolic energy during periods of inflammation.

Sarcoidosis is an inflammatory disease with cardiac involvement, causing death in 25% of affected patients (Doughan and Williams, 2006). A positive result via endomyocardial biopsy can confirm diagnosis but this technique shows low sensitivity (Hulten et al., 2016) as well as exposing the patient to an invasive procedure. MRI is commonly used for imaging patients with cardiac sarcoidosis but, alone, is not diagnostic and is not suitable for patients with implanted cardiac devices or late stage renal disease. However, PET can be used in such patients and also offers a wider field of view, potentially detecting other sites of active sarcoidosis. PET may be used alone or in

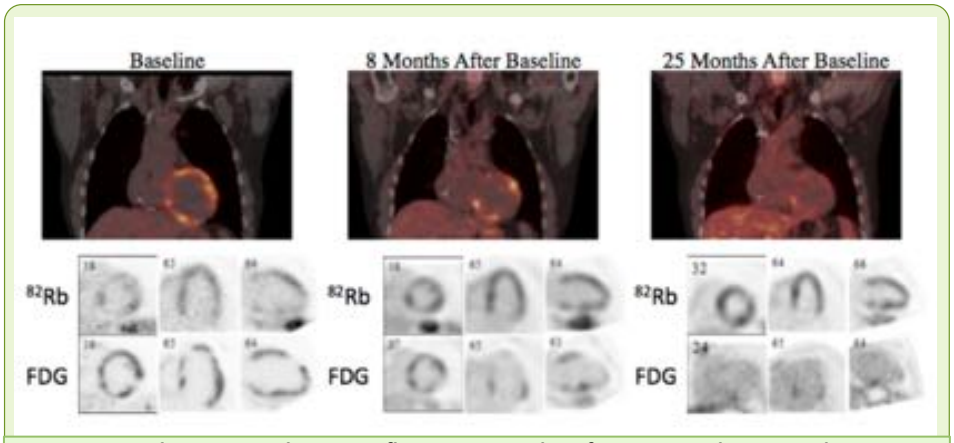

Figure 12. Serial PET scans showing inflammation and perfusion in cardiac sarcoidosis. Images are of three serial studies over 25 months in a 46-year old man with cardiac sarcoidosis treated with corticosteroids. The colour maps demonstrate the intensity of ^{18}F-FDG uptake in a coronal view. The grayscale images demonstrate serial perfusion images using ^{82}-Rubidium (top) and metabolic activity using ^{18}F-FDG (bottom) in three distinct axes at approximately the same location. Values for LV ejection fraction, SUV maximum and SUV volumes are displayed. Perfusion increased and inflammation decreased over the duration of treatment and is associated with improved cardiac performance. LV = left ventricle, SUV = standardized uptake values. Reprinted by permission from: Springer Nature, Journal of Nuclear Cardiology, 21(1), 166–174, Osborne et al., 2014.

combination with MRI for diagnosing cardiac sarcoidosis and monitoring response to treatment. Figure 12 shows how PET can be used to detect inflammation via ^{18}F-FDG and perfusion deficits via ^{82}Rb (Osborne et al., 2014). MRI is used to detect fibrosis in cardiac sarcoidosis via late gadolinium enhancement (LGE). It would be beneficial to compare this detection method with FDG-PET in larger patient trials to determine if FDG-PET can detect inflammation at the onset of pathology, prior to scar tissue formation. As shown in Figure 12, PET can also be very useful at monitoring the response to anti-inflammatory drugs, such as corticosteroids.

Interestingly, when radiologists examine PET scans for malignancies, focal uptake of ^{18}F-FDG can be observed within the larger arteries such as aorta and carotids. This uptake represents accumulation of FDG by macrophages within the walls of atherosclerotic arteries. However, PET is not used for diagnosing or monitoring atherosclerosis, despite a wide range of human studies showing potential for PET in detecting atherosclerotic plaques (MacRitchie et al., 2020a). One such example is shown in Figure 13, derived from a study by Marnane et al., 2012 designed to assess if ^{18}F-FDG-PET imaging of carotid arteries could be used to predict recurrent stroke. In the study, patients who had a recent stroke or transient ischaemic attack (TIA) were imaged via PET-CT

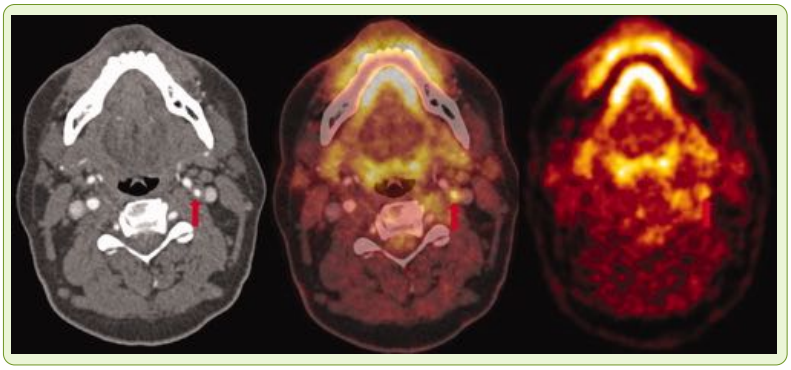

Figure 13. ^{18}F-FDG-PET-CT imaging of carotid atherosclerosis as a predictor of recurrent stroke. Left to right: Contrast-enhanced CT, fused PET-CT, PET. Arrow indicates an inflamed carotid artery that would later be causative of a recurrent stroke. Reproduced from Marnane et al., 2012. Reprinted by permission from John Wiley & Sons, Inc.

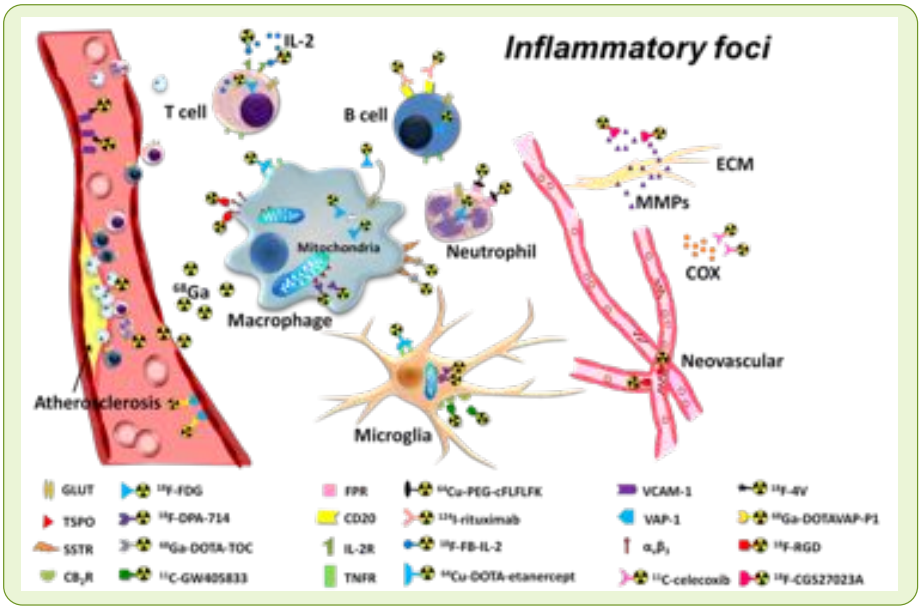

Figure 14. Examples of PET tracers and their inflammatory targets. Reproduced from: Wu et al., 2013, distributed under the terms of a Creative Commons Attribution (CC BY) license.

following ^{18}F-FDG administration. Sixty patients were assessed of which 13 had a stroke recurrence within 90 days. FDG uptake was a strong independent predictor of recurrent stroke with the highest uptake values found in patients with early recurrent stroke. Neither patient age nor stenosis values were found to be significantly predictive. Therefore, FDG-PET could have clinical use for identifying patients at high risk of recurrent stroke.

While ^{18}F-FDG remains central to current PET imaging, pre-clinically a multitude of novel targeted radiolabelled tracers have been developed, many of which target inflammatory molecules; examples of these are shown in Figure 14. The vast majority of these imaging agents are small molecules, but the first PET based NP for imaging CVD is currently in a phase 1 trial for monitoring carotid atherosclerosis (ClinicalTrials.gov: Identifier: NCT02417688). The NP (^{64}Cu-25%-CANF-Comb) is a copolymer-based agent targeted against natriuretic peptide receptor C (NPRC). PET imaging of CVD utilising radioligands targeted to translocator protein (TSPO) (Lamare et al., 2011; Gulyas et al., 2012) and somatostatin receptors (SSTRs) (Pedersen et al., 2015; Tarkin et al., 2017) are two notable examples where in-human trials have shown positive results in detecting cardiovascular inflammation. Indeed, the SSTR ligand, ^{68}Ga-DOTATATE was found to be superior to ^{18}F-FDG in discriminating high risk from low risk coronary lesions (Tarkin et al., 2017). However, tracer availability and poor signal to noise in the myocardium remain obstacles to their clinical use. CXCR4 is also a promising target for cardiovascular PET since CXCR4 expressing immune cells increase in density within atherosclerotic plaques as the disease progresses. Utilising ^{68}Ga-pentixafor, a radioligand that has shown promise in animal models and small human trials for detecting abnormalities within the vasculature (Hyafil et al., 2017; Li et al., 2018), Weiberg et al., 2018 employed a retrospective analysis of patients scanned with ^{68}Ga-pentixafor for non-cardiovascular related conditions and discovered that ^{68}Ga-pentixafor

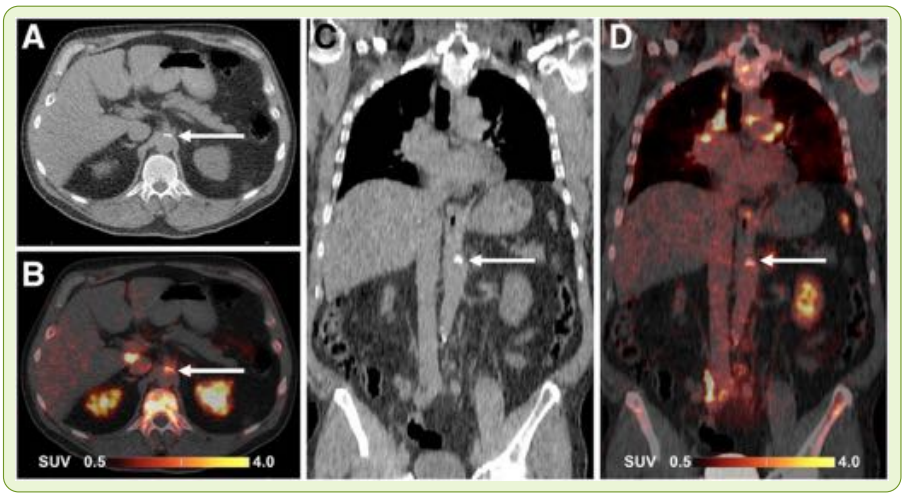

Figure 15. ^{68}Ga-pentixafor PET/CT images of abdominal aorta in 64-y-old man. CT (A and C) and PET-CT (B and D) images in transaxial (A and B) and coronal (C and D) views show ^{68}Ga-pentixafor uptake in calcified atherosclerotic lesion (arrows) coincident with calcification. Reproduced from Weiberg et al., 2018. Copyright of the Society of Nuclear Medicine and Molecular Imaging (SNMMI).

binding was significantly associated with plaque burden, the presence of CVD risk factors and prior major adverse cardiovascular events (MACE). The strongest ^{68}Ga-pentixafor signal was found in later stage calcified lesions (Figure 15). Given the favourable properties of ^{68}Ga-pentixafor (low nanomolar affinity, low background in adjacent tissues, rapid renal excretion, patients do not require a pre-scan fast and synthesis which does not require an on-site cyclotron), it may offer an alternative to ^{18}F-FDG, particularly for imaging coronary vessels where its superior specificity is more critical. It will also be important going forward to identify the cellular source of ^{68}Ga-pentixafor binding within the inflamed vessel.

Figure 16 illustrates how PET compares to our ideal molecular imaging tool from Figure 3. The great strength of PET (and nuclear imaging in general) is superior sensitivity over other clinical imaging modalities. This allows for only trace amounts of radionucleotides to be used thus reducing radiation burden for the patient. PET also allows for body wide imaging and when combined with CT (PET-CT) or MRI (PET-MRI) then anatomic information can also be produced which facilitates more accurate detection and quantification. The use of standardized uptake values (SUVs) allows for quantification, although in many instances the outcome can only be described as semi-quantitative. The major technical limitation of PET is poor spatial resolution, currently in the region of 4-6 mm clinically and 1-2 mm pre-clinically (MacRitchie et al., 2020a). This is sufficient only to detect gross accumulations of inflammatory cells, or a large number of receptors expressed, for example on inflamed endothelium. Another limitation is the lack of multiplexing capability which is a severe restriction in building up information on the multiple inflammatory cells and markers that are present within inflamed tissue. FDG is just one piece of information, linking areas of hyper-metabolism to increased phagocytic activity. For example, it does not distinguish between different macrophage subtypes or other highly metabolically active immune cells. Finally, PET is extremely high cost with PET scanners and maintenance costs running to many millions of pounds and certain tracers (due to

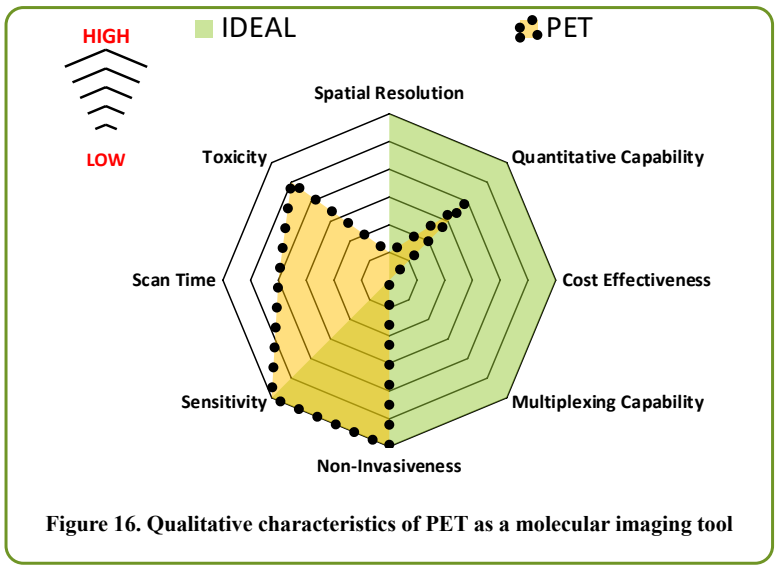

Figure 16. Qualitative characteristics of PET as a molecular imaging tool

short half-lives) also require an on-site cyclotron or geographical closeness to such a facility. These are some of the critical reasons why PET is not more widely used. The use of PET for imaging out with oncology has to be carefully considered in relation to the high cost versus potential patient/clinical gain (See section on barriers to translation).

Contrast Enhanced Ultrasound (CEUS)

Given the limitations of MRI and PET such as long imaging times and high cost, the question arises: is there a faster cheaper alternative for molecular imaging? Ultrasound (US) is routinely used in the clinical for detecting morphological and perfusion changes in tissue. While most US is performed non-invasively, the use of catheter-based US devices are often used for high resolution scanning of the interior wall of arteries (intravascular ultrasound, IVUS). Like CT and MRI, the use of contrast agents improves the resolution and sensitivity of US and CEUS is frequently used for imaging heart and blood vessel abnormalities. All clinically approved contrast agents are microbubbles which are up to 8 µm in size (therefore confining them to the vasculature for imaging) and have an excellent safety profile in humans (Schinkel et al., 2016). Microbubbles do not require a long delay post-injection before imaging can begin (typically a few minutes) and offer real-time feedback to the sonographer. While clinical imaging exclusively utilised microbubbles, pre-clinically, other imaging agents are utilised including smaller nanoscale liposomes and NPs. Advantages of these agents is that imaging is not confined to the vasculature and can be tuned more easily for different experimental requirements. While pre-clinical imaging agents are often targeted to various markers of inflammation or other disease related molecules, clinically utilised microbubbles are all non-targeted. However, the feasibility of using targeted microbubbles in patients was proven in a successful clinical trial using a clinical-grade kinase insert domain receptor (KDR) targeted microbubble (BR55) for detecting

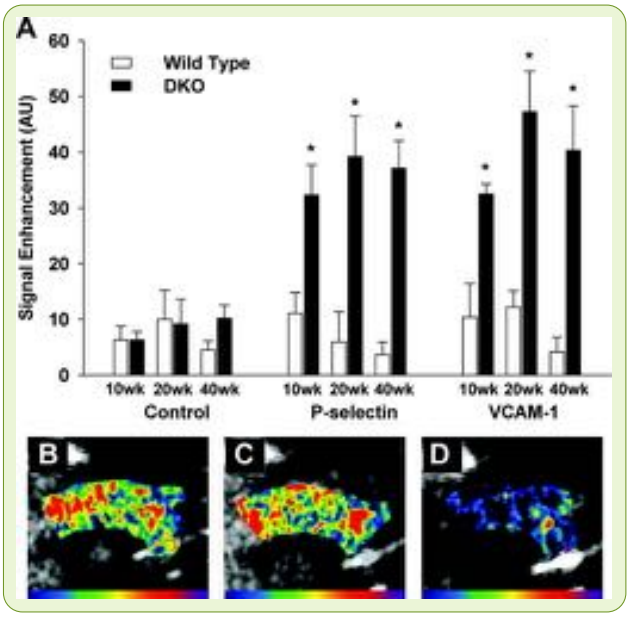

Figure 17. CEUS imaging of the aortic arch in a mouse model of atherosclerosis. LDLR$^{-/-}$Apobec-1$^{-/-}$ (DKO) or control mice were injected with anti-P-selectin targeted, VCAM-1 targeted or control microbubbles and imaged 10 minutes later. Data is presented as mean (+/- SEM) background subtracted signal intensity in the proximal aorta. * P<0.05. N = 7-10. Reproduced from Kaufmann et al., 2010. Arteriosclerosis, Thrombosis, and Vascular Biology, 30(1), 54–59. Reprinted with permission from Wolters Kluwer Health, Inc. and American Heart Association, Inc.

the presence of breast and ovarian cancer (Willmann et al., 2017). Importantly, the safety profile of BR55 was similar to a non-targeted microbubble (Schneider et al., 2011). It would be hoped that such results will lead to more clinical trials for CEUS utilising microbubbles targeted against disease markers.

With microbubbles being restricted to the circulation, endothelial markers of inflammation are particularly attractive for CEUS cardiovascular imaging. Figures 17 and 18 are two examples from animal models of how microbubbles may be used to target early and late markers of cardiovascular pathology respectively. Figure 17 illustrates how microbubbles can be used to detect endothelial activation using anti-P-selectin and anti-Vascular cell adhesion protein 1 (VCAM-1) targeted microbubbles (Kaufmann et al., 2010). Since endothelial activation is an early sign of endothelial injury and can precede formation of fatty streaks in atherosclerosis, these targets may be important in early detection of vascular abnormalities.

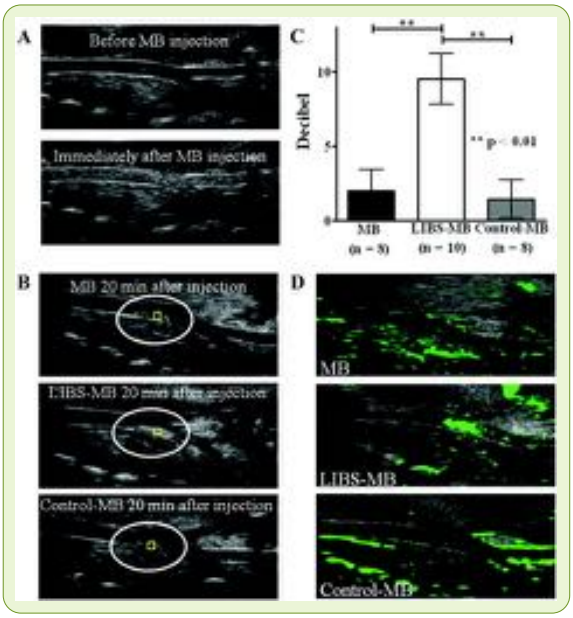

Figure 18. CEUS imaging of left carotid thrombi in mice. (**A**) Representative US images of mouse carotid artery before and after microbubble (MB) injection. (**B**) Representative US images, taken in real-time, of a carotid thrombus 20 mins after injection of untargeted MBs, microbubbles targeted to glycoprotein IIB/IIIA (LIBS-MB) and a microbubble conjugated to a mutated version of the antibody targeting ligand (Control-MB). The brightening of the image shows the binding of LIBS-MB which contrasts with MB and control-MB groups where signal intensity is lower. (**C**) Decibel levels show LIBS-MS produced a significant increase in intensity with respect to control groups. (**D**) Following analysis with digital subtraction, areas which appeared brighter than the reference image are shown in green. Only the LIBS-MB treated animals showed strong intensity of staining at the site of thrombi. Reproduced from Wang et al., 2012, Circulation, 125(25), 3117–3126. Reprinted with permission from Wolters Kluwer Health, Inc. and American Heart Association, Inc.

In contrast, Wang et al., 2012 developed microbubbles conjugated with antibody fragments targeted against glycoprotein IIB/IIIA, which is present only on activated platelets and thus allows detection of thrombi, a key feature of chronic vascular injury. Figure 18 shows example US images taken from a study employing these microbubbles in a mouse model of carotid injury. Notably, in this study, the authors were also able to use these same targeted microbubbles to assess the efficacy of urokinase thrombolytic therapy. Such a simple real-time monitoring of therapeutic efficacy would be very appealing in a clinical setting.

One CVD that would greatly benefit from non-invasive molecular imaging is myocarditis, a disease characterised by aberrant inflammation of the myocardium, most commonly due to viral infection. While biopsy is routinely performed in suspected cases, diagnostic sensitivity can be poor due to the diverse presentation of the

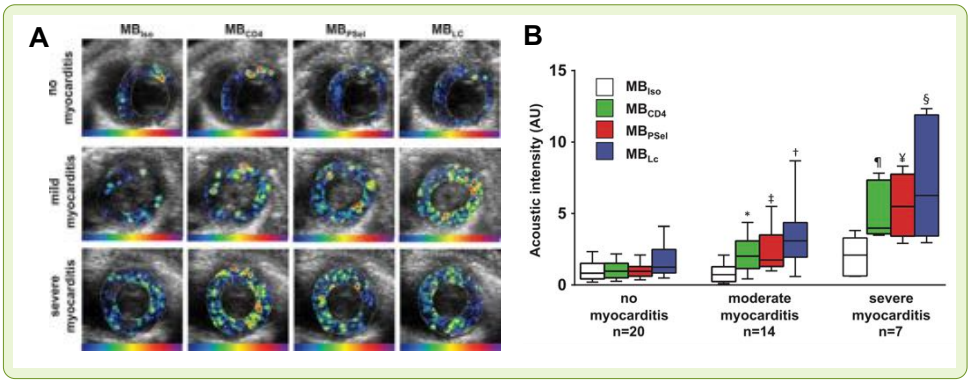

Figure 19. Ultrasound imaging in a mouse model of myocarditis. (**A**) Representative false colour US image in animals with no myocarditis (top), mild myocarditis (middle) or severe myocarditis (bottom). Each animal received CD4 targeted (MB_{CD4}), P-selectin targeted (MB_{pSel}), total leukocyte targeted (MB_{LC}) or isotype targeted (MSiso) microbubbles in a random order in a sequential manner. (**B**) Acoustic intensity values for targeted and isotype control microbubbles. Data are median values (horizontal line), 25% to 75% percentiles (box) and range of values (whiskers) of the video intensity. *P = 0.027, ‡P = 0.0133, †P = 0.0004, ¶P = 0.0381, ¥P = 0.0192, §P = 0.0073 vs MBIso in the same animal group. Reproduced from Steinl et al., 2016, Circulation. Cardiovascular imaging, 9(8), e004720. Reprinted with permission from Wolters Kluwer Health, Inc. and American Heart Association, Inc.

disease (Van Linthout and Tschöpe, 2018) and multiple biopsies of both ventricles may be required. Utilising a mouse model of myocarditis, Steinl et al., 2016 employed 4 'flavours' of microbubbles to image inflammation within the heart using US (Figure 19). Using CEUS, the authors could detect the presence of P-selectin, CD4+ T cells and total leukocytes with signal intensity correlating with disease severity. The rapid elimination/destruction of microbubbles allows sequential imaging with microbubbles with affinity for a different target. While not multiplexing in the strictest sense, it does allow significantly more information to be gained on the current inflammatory state than what could be achieved with nuclear imaging where radiotoxicity and long scans would preclude repeat imaging.

Figure 20 illustrates how CEUS compares to our ideal molecular imaging tool from Figure 3. For regulatory approval and adoption by healthcare authorities, the top and bottom aspects of the wheel will feature strongly, namely low toxicity and low cost. In both these regards, US compares very favourably with other modalities. As mentioned above, microbubbles have a

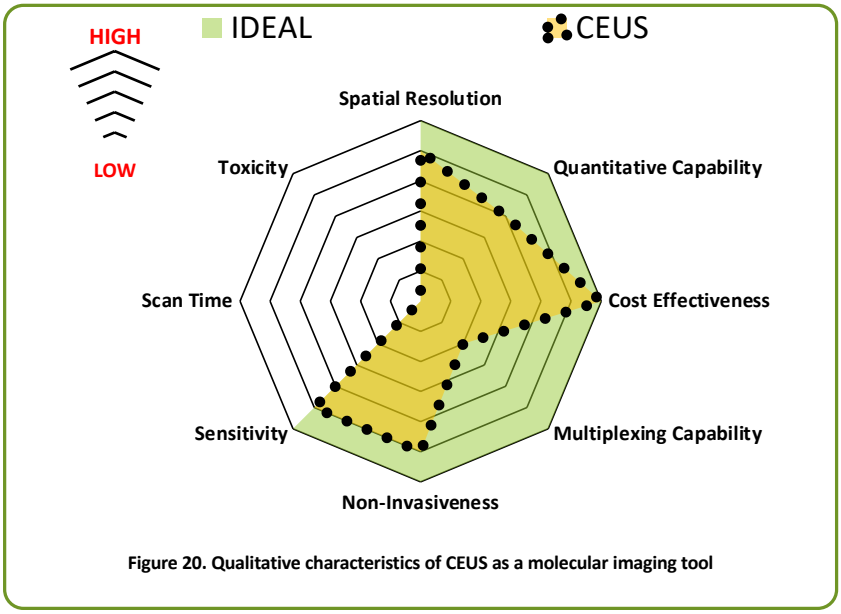

Figure 20. Qualitative characteristics of CEUS as a molecular imaging tool

long history of use in humans and minor changes to the surface with targeting ligands, particularly small molecules with low immunogenicity, are unlikely to significantly alter this safety profile. However, we only have one example (BR55) where safety data is available, but it is a promising start. US also provides real-time (or near real-time) imaging and scanning can begin in just a few minutes after microbubble injection as opposed to an hour or more with PET. Spatial resolution also compares favourably with MRI and CT and sensitivity is higher than both. In the cancer study with BR55, the dose of BR55 was similar to doses typically used where non-targeted microbubbles are used. Such a dose was clearly sufficient to detect tumour specific biomarkers with precision. Several methods exist for quantification such as the destruction-replenishment method (Abou-Elkacem et al., 2015), a pre-requisite for reproducible clinical data. Finally, CEUS does not allow for multiplexing, that is the simultaneous acquisition of signal from multiple imaging agents in a single scan. There is no clear path to separate the signal of differently targeted microbubbles. However, the rapid elimination of microbubbles from the circulation (Willmann et al., 2008), coupled with the low toxicity, means sequential scans could be performed in the same patient using microbubbles with a different molecular target to build up more information on which cells and inflammatory markers are presented at the site of interest. This is one of the major goals of molecular imaging and would greatly aid clinical decision making, particularly if such multiplexed scans can be performed repeatedly to monitor disease progression/response to therapy.

Near-Infrared Fluorescence (NIRF)

NIRF is primarily a pre-clinical research tool for understanding the cellular and molecular processes of disease states. However, promising developments are being made in invasive catheter-based approaches where the great strengths of fluorescence-based imaging can be combined with current technologies such as optical coherence tomography (OCT) or IVUS to improve our understanding of the molecular changes within the vessel wall. As will be discussed in this section, the key limitations of NIRF (namely lack of tissue penetration) makes non-invasive molecular imaging out of reach with current technologies. In the clinic, the only routinely used fluorescence contrast agent is indocyanine green (ICG). It is used for invasive detection of tumours, guiding surgery, lymph node mapping and monitoring hepatic function (DSouza et al., 2016; Kahramangil and Berber, 2017) but has no current use for imaging inflammation.

NIRF, as the name implies, utilises the near-infrared spectrum (650-1000 nm) for imaging. Within this wavelength window, there is less tissue absorption of photons and less autofluorescence. However, light scattering and absorption means the ability to acquire high resolution images decreases substantially as tissue depth increases. Therefore, while ICG may be used to detect a tumour (of several cm diameter) at a depth of 2 cm, for cellular or molecular imaging, NIRF is restricted to around 1 mm depth depending on the optical properties of the tracer and tissue, laser strength and acquisition time (Scales et al., 2016). The smaller size of rodents coupled with less restrictions on laser power and the use of alternative materials for increased brightness has led to some very interesting studies emerging that utilise NIRF imaging for detecting the presence of vascular pathology. In one such study, Lim et al., 2017 used a 3D optical imaging system known as FLECT (fluorescence emission computed tomography) in combination with nano-CT to image vascular thrombosis in mice. The fluorescent probe was a Cy7 dye labelled antibody fragment that binds only to activated platelets, thus allowing detection of thrombosis *in vivo*. Some of these results are presented in Figure 21. Moreover, in other results Targ-Cy7 could also be used with FLECT to monitor resolution of thrombus following thrombolytic therapy. At present, FLECT and other fluorescence-based detection methods are not at the level of sensitivity to be used non-invasively on patients since the heart and vasculature are too deep for current technology. However, great advances are being made in improving imaging depths, signal to noise and reducing autofluorescence. In the short term, it is far more probable

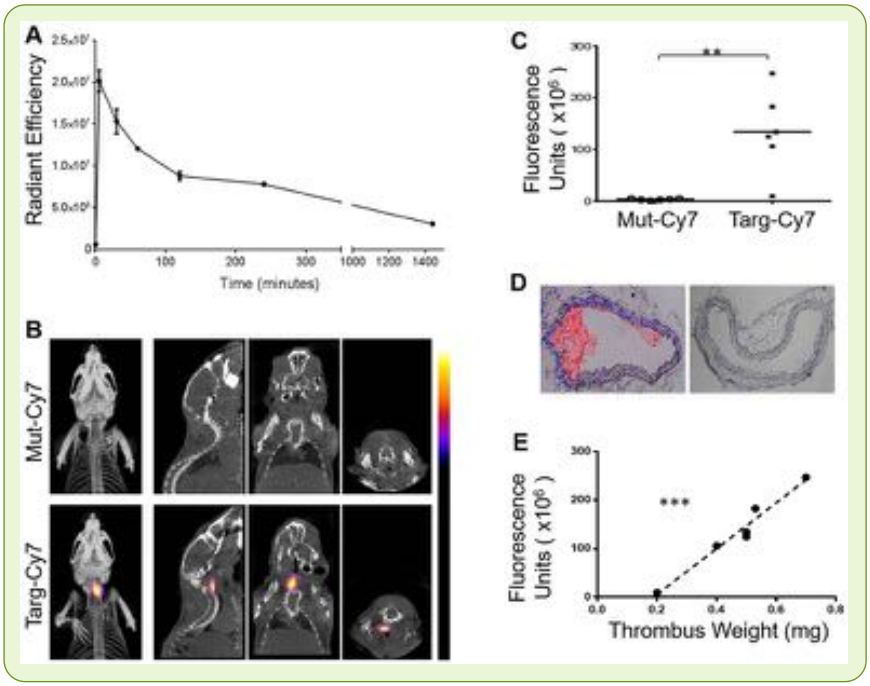

Figure 21. FLECT/CT of Targ-7 in mice with left carotid thrombosis. (**A**) Residence times of the probe with 50% remaining at 96 minutes. (**B**) Left carotid arteries of mice were exposed to ferric chloride to induce injury and mice were injected with either a Cy7 Ab chain targeted against activated platelets (Targ-Cy7) or a mutated control (Mut-Cy7) and imaged on the FLECT/CT scanner. The intensity of the NIRF is greatest in white areas and lowest in blue. N = 6 per group. (**C**) Quantification of results obtained from FLECT/CT imaging showing significantly higher fluorescence intensity in mice injected with the Targ-Cy7 probe. (**D**) Representative images showing ferric chloride injured artery (left) and uninjured contralateral artery (right). Blue colour is nuclear DAPI staining and Red is platelet specific CD41. (**E**) FLECT signal shows a highly significant correlation with weight of thrombus. Reproduced from: Lim et al., 2017, distributed under a Creative Commons Attribution (CC BY-NC) license.

that clinical fluorescence-based imaging approaches are going to take the form of multi modal invasive systems such as dual OCT-NIRF or IVUS-NIRF catheters for molecular mapping of vessel walls. Indeed, the use of NIRF catheters combined with OCT has been trialled on human patients following injection with ICG and while excised carotid plaques showed significantly enhanced uptake of ICG (Verjans et al., 2016), ICG is taken up non-specifically with high variability and therefore, it is debatable whether this approach is more informative than current standalone imaging techniques. To avoid the barrier of requiring regulatory approval for a novel fluorescent imaging agent, some researchers have focused on detecting fluorescence from endogenous molecules in the body. In a study by Ughi et al., 2016 (Figures 22, 23) OCT-near-infrared fluorescence to detect artery wall autofluorescence (NIRAF) imaging was performed in patients undergoing percutaneous coronary intervention (PCI). An overview of the scanning procedure is shown in Figure 22. As shown in Figure 23, NIRAF was detected at areas where plaque rupture/thrombosis formation occurred (Ughi et al., 2016). Researchers are keen to determine the exact source of autofluorescence within injured/diseased arteries. Studies have suggested that bilirubin, a blood breakdown product could be a major source of autofluorescence in plaques with intraplaque haemorrhage (Htun et al., 2017). However, bilirubin is unlikely to be the only source with several other auto-fluorescent molecules such as modified lipoproteins contributing. In the study by Ughi et al., 2016, OCT revealed that NIRAF was only detected in regions that resembled macrophage aggregates, suggesting a link between plaque autofluorescence and inflammation. It will be interesting to characterise the optical properties of the various auto-fluorescent species within cardiovascular lesions to determine if different molecular optical

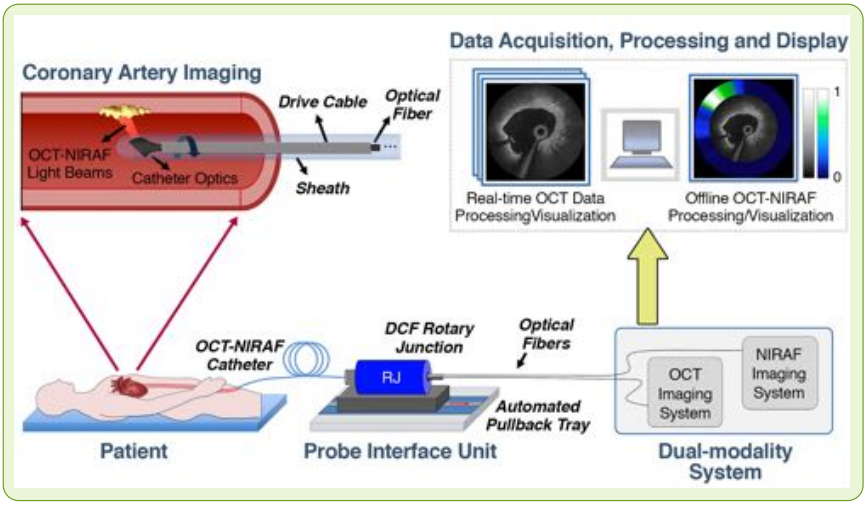

Figure 22. Schematic of the OCT-NIRAF system. OCT-NIRAF imaging was performed using a dual OCT-NIRAF catheter placed into the coronary artery of patients undergoing percutaneous coronary intervention (PCI). The mechanical procedure is fundamentally the same as standalone OCT. Dual imaging is accomplished by focusing OCT and NIRAF excitation light from the catheter tip to the arterial wall. The probe can image at 100 frames per second and NIRAF is detected using an excitation wavelength of 633 nm with signal acquisition in the 675-900 nm window. Three-dimensional OCT and NIRAF images are obtained simultaneously, collected by computer and processed. OCT data is displayed in real time whereas NIRAF data is processed and displayed offline as two dimensional NIRAF maps and as dual-modality OCT-NIRAF images. Reprinted from Ughi et al., 2016, JACC. Cardiovascular Imaging, 9(11), 1304–1314, with permission from Elsevier.

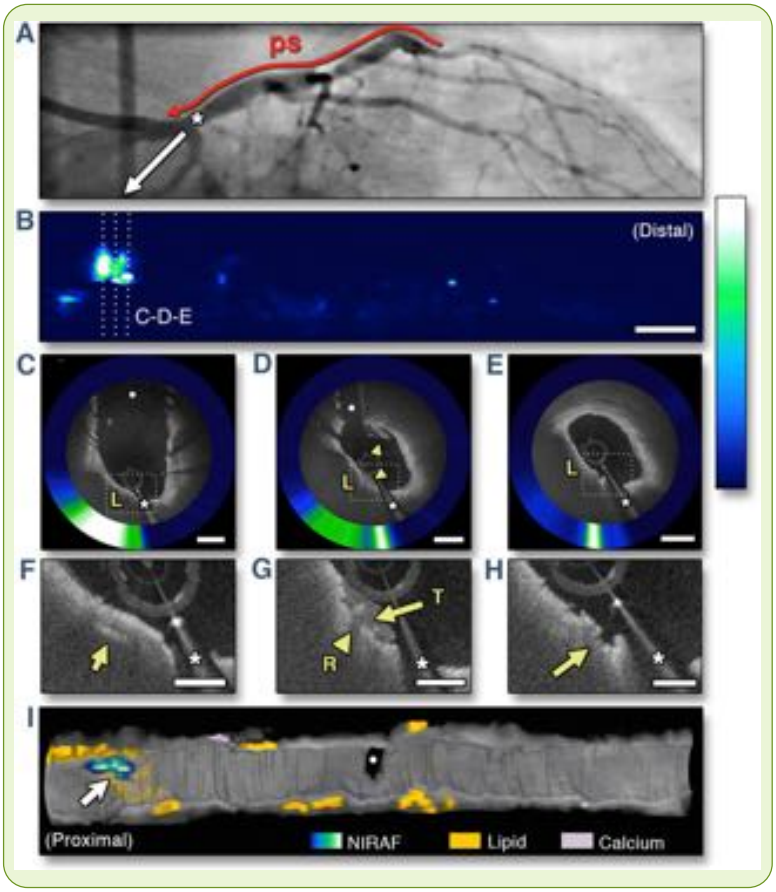

Figure 23. OCT-NIRAF Imaging of TCFA Rupture. (**A**) Angiogram of the left anterior descending coronary artery (LAD). (**B**) Distal view of the LAD showing focal areas of NIRAF. (**C-E**) show cross sections from the site shown in (**B**). (**D,G**) show a platelet rich thrombus over the rupture site. The rupture site in **G**, indicated by arrowhead is shown adjacent to thrombus. (**E,H**) TCFA rupture site co-localizes with highest NIRAF. Arrowhead in (H) points to TCFA rupture. * = guidewire shadow; ps = pullback segment; L = lipid; R = rupture site; T = thrombus; TCFA = thin cap fibroatheroma. Reprinted from Ughi et al., 2016, JACC. Cardiovascular Imaging, 9(11), 1304–1314, with permission from Elsevier.

signatures can be used to stage lesions or if molecules with sufficiently different optical properties can be detected simultaneously for more informative multiplexed imaging. Considering the ease of adaptation of clinically used OCT catheters and the lack of requirement for exogenous imaging agents, a label free approach such as described here has significantly fewer barriers to translation than other modalities that rely on imaging agents with only pre-clinical testing or that are limited by toxicity.

The great strengths of NIRF imaging are high spatial resolution and sub-nanomolar sensitivity (Figure 24). Toxicity depends, to some degree on laser strength but of much greater importance is the composition of the imaging agent. While some quantum dots (QDs), (known for their favourable optical properties) show low toxicity in rodents (Hong et al., 2012) and may ultimately be safe in

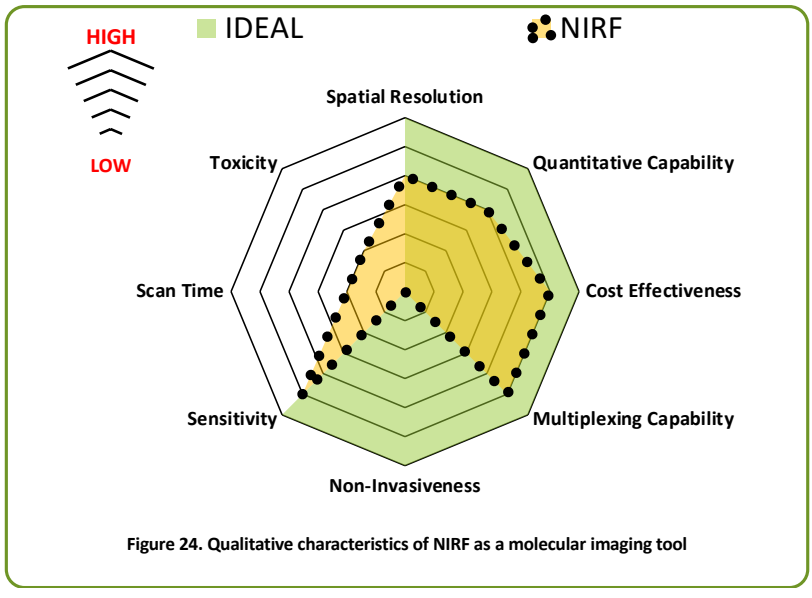

Figure 24. Qualitative characteristics of NIRF as a molecular imaging tool

humans, others, including some of the brightest QDs, contain heavy metals which would preclude their clinical use (Bruns et al., 2017). QDs with narrow emission spectrums are well placed for multiplexing where spectral unmixing of multiple fluorophores (excited at multiple wavelengths) would be possible. However, since imaging is restricted to only a few mm of tissue at present, it is likely invasive catheter based approaches will be the only near to medium term route to the clinic for imaging the cardiovascular system, likely supplementing data obtained by OCT or IVUS as described in the example above.

Photoacoustic Imaging (PAI) and Multi-spectral Optical Tomography (MSOT)

PAI, as the name implies, uses a combination of optical and acoustic properties to create an image. Briefly, PAI utilises short wavelength optical pulses to generate acoustic energy of endogenous molecules or external tracers that can be detected by US transducers. PAI uses non-ionizing radiation and US detection, which allows much deeper imaging than NIRF imaging. Melanin and haemoglobin are the main molecules of interest for endogenous PAI. PAI can determine the oxygenation state of haemoglobin which can be used to determine changes in perfusion and active inflammation. While no exogenous contrast agents are approved for clinical use, pre-clinically, exogenous photoacoustic compatible tracers include strong light absorbing NPs that greatly increase the sensitivity and depth of imaging while also allowing targeted molecular imaging. The use of NPs in PAI has seen significant performance increases over the last 15 years with sensitivity of detection down to the picomolar range (de la Zerda et al., 2012). Like NIRF imaging, NPs may be organic or inorganic based and depending on their properties, can be used for multiplexing, even in combination with endogenous molecules.

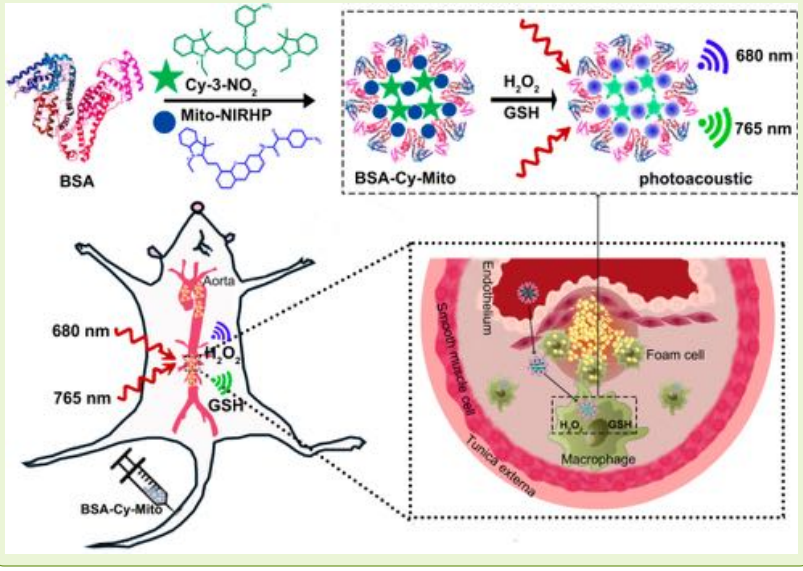

Figure 25. Schematic showing structure of GSH/H_2O_2-responsive BSA-Cy-Mito nanoprobe and functional use in PAI in vivo imaging to monitor the redox status of atherosclerotic plaques in apoE$^{-/-}$ mice. Reproduced from Gao et al., 2019, Analytical chemistry, 91(1), 1150–1156. Copyright American Chemical Society.

Figures 25 and 26 are taken from an elegant study where PAI is used to determine the level of oxidative stress present within atherosclerotic lesions (Gao et al., 2019). A BSA-stabilised nanoprobe (BSA-Cy-Mito) was created containing two fluorescent probes, one (Cy-3-NO_2) for glutathione (GSH) and the other (mito-NIRHP) for hydrogen peroxide (H_2O_2), each with distinct absorption wavelengths of 765 and 680 nm, thus allowing simultaneous detection of GSH/H_2O_2 and therefore the redox status of the plaque. Both probes have sub micro-molar sensitivity, display 10-hour half-lives and show peak accumulation within the plaques of apoE$^{-/-}$ mice at 2 hours following injection. As shown in Figure 26, increasing severity of atherosclerosis resulted in a greater H_2O_2 signal concomitant with decreasing GSH signal, indicating that PAI can detect redox changes that correspond to plaque severity. H_2O_2 detection was most pronounced in advanced plaques in areas of strong lipid and macrophage staining. Interestingly, *in vitro* studies with ox-LDL stimulated macrophages also showed an enhancement of H_2O_2 signal with decreased GSH signal. Therefore, PAI in combination with BSA-Cy-Mito can detect inflammatory activity in atherosclerotic plaques via changes in GSH/H_2O_2 ratio.

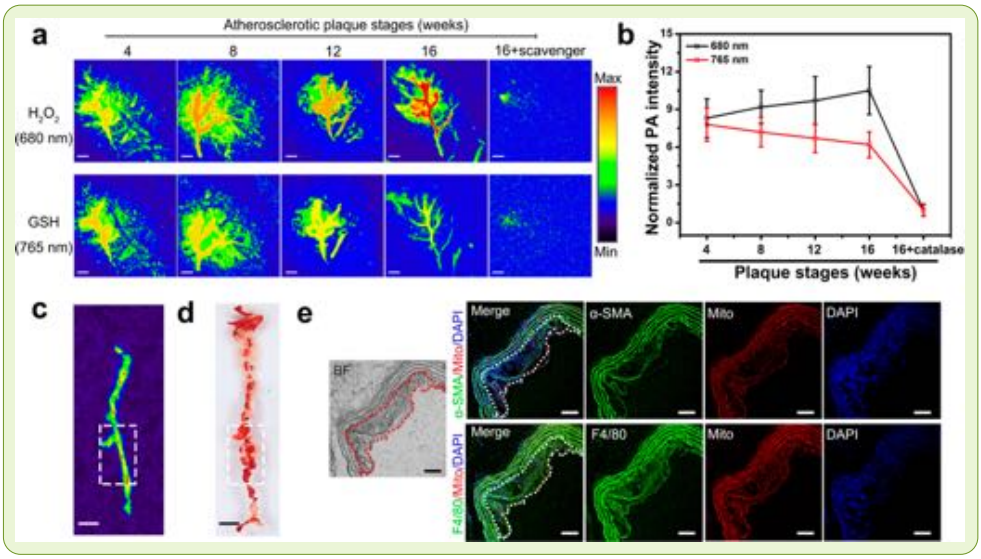

Figure 26. *In vivo* PAI of atherosclerotic plaque in apoE$^{-/-}$ mice. (**A**) PAI of abdominal aortas at different stages of pathology following BSA-Cy-Mito injection (10 mg/kg). Some mice were also treated with scavengers (catalase for H_2O_2 and BSO for GSH). Scale bar = 2 mm. (**B**) Normalized photoacoustic (PA) signal derived from (**A**). Data shown as mean ± SD (n = 3). (**C**) Representative *ex vivo* PAI of the aorta from 16 weeks high fat diet fed mice. Scale bar = 5 mm. (**D**) Representative images of atherosclerotic lesions stained with Oil-Red-O. White dashed lines represent abdominal aorta. Scale bar = 5 mm. (**E**) Bright field and immunofluorescent images of aortic plaque cross sections in mice fed high fat diet for 16 weeks. Dashed line indicates lesion border. Scale bar = 100 µm. Reproduced from Gao et al., 2019, Analytical chemistry, 91(1), 1150–1156. Copyright American Chemical Society.

Photoacoustic scanners are currently being trialled as an alternative (or adjunct) to X-ray mammography and US for breast cancer detection (Valluru et al., 2016; Steinberg et al., 2019). Furthermore, PAI is showing promise in human trials for imaging inflammatory conditions such as rheumatoid arthritis (Jo et al., 2017). These trials involve resolving changes in vasculature perfusion or oxygenation state via changes in haemoglobin as described above.

Studies in breast cancer have shown that PAI has a spatial resolution of 250 µm at a depth of 4 cm, allowing visualisation of even small tumours. This level of depth and spatial resolution also makes imaging superficial vessels such as the carotid artery possible. Indeed, PAI has already been applied to imaging the carotid artery in people (Ivankovic et al., 2019). Figure 27 shows how a handheld multispectral optoacoustic tomographic (MSOT) scanner was used for real-time imaging of the carotid artery with a spatial resolution of ~200 µm, a depth of several cms, with a field of view of 2 cm^3. The scanning procedure was performed on 16 healthy volunteers. Analogous to breast imaging, the optoacoustic signal is generated primarily by haemoglobin thus allowing the discernment of arterial structure. Imaging with the handheld scanner was performed at either 850 or 1064 nm with the 1064 nm near-infrared scanning achieving the best image contrast, due to the higher signal intensity of oxygenated haemoglobin at this wavelength. In contrast, deoxygenated haemoglobin showed a higher intensity at the shorter wavelength. Importantly, this proof of concept study showed that the architecture of the carotid artery could be more readily visualised compared with a clinical B-mode US scanner and that no adverse events were reported by study participants. Therefore, by generating images acquired from data derived from mostly one type of molecule, it is possible to resolve the gross structural features of the carotid artery in a non-invasive manner.

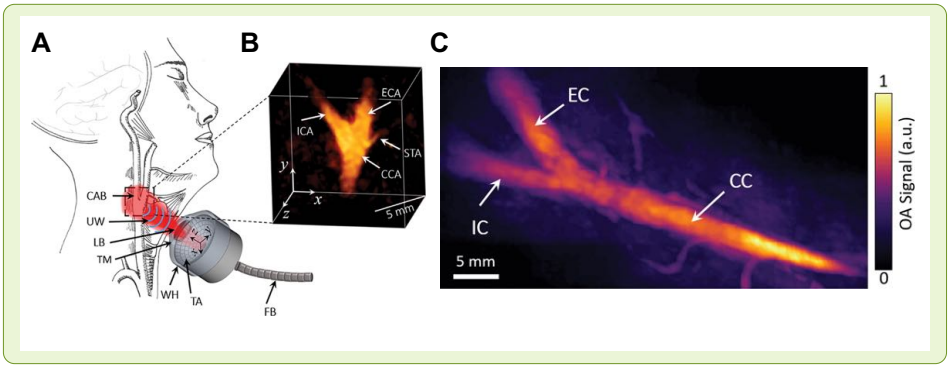

Figure 27. Multispectral optoacoustic tomographic (MSOT) imaging of the carotid artery. (**A**) Schematic showing the use of a handheld MSOT scanner for non-invasive volumetric imaging of carotid artery bifurcation. (**B**) Three dimensional MSOT image of carotid bifurcation in a 44-year-old man. (**C**) Compounded image of MSOT scan along entire carotid artery in a 26-year-old woman. CAB = carotid artery bifurcation, CCA = common carotid artery, ECA = external carotid artery, FB = fibre bundle, ICA = internal carotid artery, LB = laser beam, STA = superior thyroid artery, TA = transducer array, TM = transparent membrane, UW = ultrasound waves, WH = water holder, CC = common carotid, EC = external carotid, IC = internal carotid. Figure and figure legend reproduced from Ivankovic et al., 2019. Permission granted by the Radiological Society of North America (RSNA®).

Photoacoustics is a promising emerging technology that offers the advantages of optical imaging such as multiplexing and high sensitivity but also of US in being able to spatially localise the signal and present real-time images. Figure 28 illustrates how PAI compares to our ideal molecular imaging tool from Figure 3. As noted above, much of the clinical testing of PAI has been in breast cancer screening. In comparison to X-ray mammography, PAI lacks

ionising radiation and offers better soft tissue discrimination. Toxicity, if limited to endogenous molecules will be low since only short exposure to laser light is required. Spatial resolution is also good, but dependent on imaging depth. As observed in the study by Ivankovic et al., 2019, spatial resolution was sub mm at the depth of the carotid artery but more superficial structures can be imaged at a resolution an order of magnitude greater (Zhang et al., 2006), thus representing an improvement over NIRF which is restricted to mm level imaging. For PAI to fulfil its potential as a molecular imaging modality in CVD, it would also be necessary to exploit its other strengths of high sensitivity and multiplexing. It has already been confirmed that PAI can detect lipids within atherosclerotic plaques (Allen et al., 2012; Kruizinga et al., 2014) and it would be interesting to see if more complex MSOT experiments could discriminate blood flow, architecture and lipid content on the wall of carotid arteries. Interestingly, lipids have been detected at 1200 nm excitation which may allow simultaneous detection of haemoglobin at 1064 nm (Ivankovic et al., 2019). For more extensive multiplexing and to increase sensitivity of molecular detection will require the use of exogenous imaging agents. Pre-clinically, there are a growing number of studies (such as that conveyed in Figures 25/26) that utilise either organic or inorganic NPs for deeper, more sensitive multiplexed imaging. In animal models, PAI has shown to be a reliable tool for detection of inflammation within the cardiovascular system. As mentioned elsewhere in this visual review, the use of NPs in human trials will likely depend on success in other areas (such as cancer therapeutic/theranostics) and using biocompatible materials, particularly those with a history of use in humans coupled with extensive pre-clinical testing (See 'Barrier to Clinical Translation' section for further details).

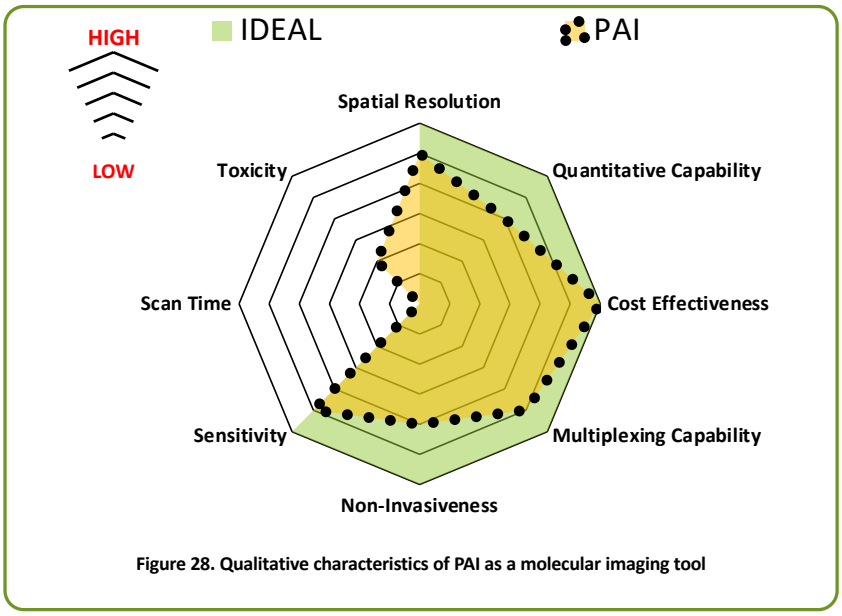

Figure 28. Qualitative characteristics of PAI as a molecular imaging tool

Surface-enhanced Raman Spectroscopy (SERS)

SERS is a form of vibrational spectroscopy and is a more sensitive form of traditional Raman

spectroscopy (Laing et al., 2017). It requires the target molecule to be in close proximity to a plasmonic metallic surface (typically gold or silver). Silver or gold-based NPs can then be functionalised with targeting molecules (peptides, aptamers, and antibodies) towards a particular marker of interest. The SERS signal in most instances is produced indirectly by the incorporation of a Raman reporter into the NP. These are molecules that can produce a strong SERS effect (Figure 29). While SERS is still in the early stages of *in vivo* imaging, it holds several striking advantages that make it amenable to molecule imaging. In our lab, we have designed human adhesion molecule-targeted SERS NPs (McQueenie et al., 2012; Noonan et al., 2018), each conjugated with an antibody with affinity towards a different adhesion molecule (ICAM-1, VCAM-1, P-selectin) plus an isotype conjugated control, with each NP type containing a unique Raman reporter for multiplex imaging.

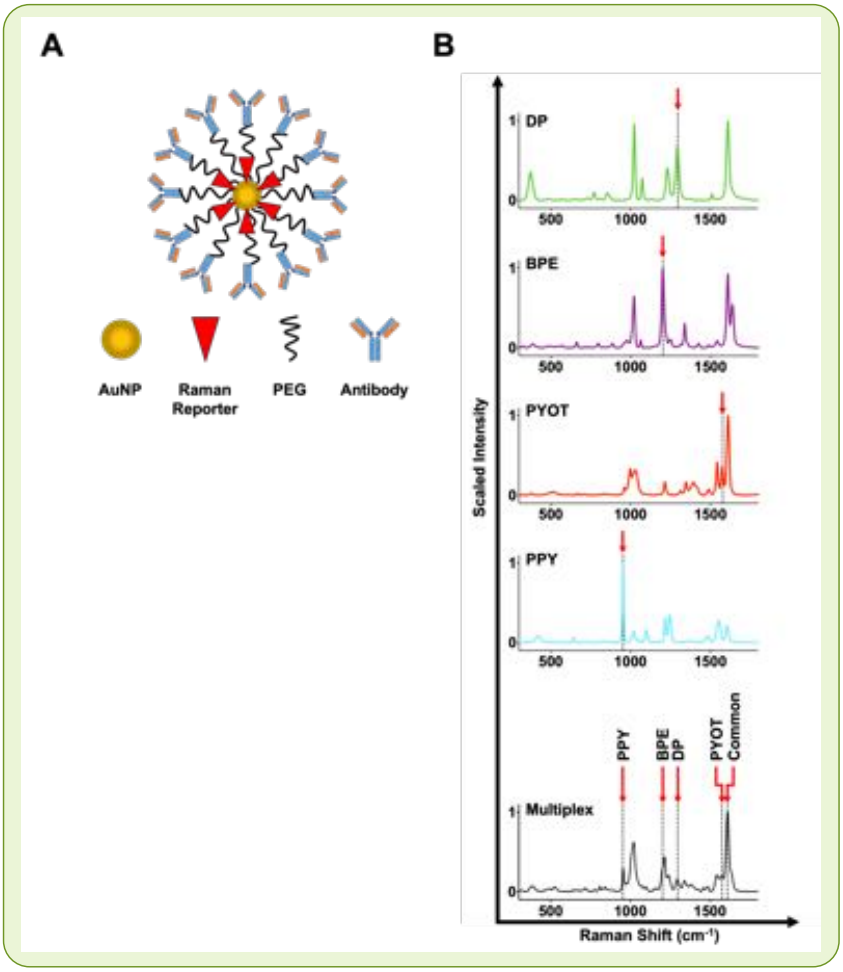

Figure 29. Design and characterisation of biofunctionalized SERS nanoparticles. (**A**) Schematic depicting a solid gold NP core (AuNP) conjugated to Raman reporter molecules; this Raman reporter covered core was then conjugated with antibody-functionalized polyethylene glycol (PEG) to increase biocompatibility and increase circulating residence times. (**B**) Raman spectrum from 4 distinct SERS NPs. From top to bottom: Isotype labelled NPs with DP Raman reporter; anti-ICAM-1 NPs with BPE Raman reporter; anti-VCAM-1 NPs with PYOT Raman reporter; anti-P-selectin NPs with PPY Raman reporter and an example of a SERS multiplex spectra containing each distinct combination. Red arrows indicate peaks unique to each Raman reporter and also a common peak present in each (1605 cm-1). Reproduced from: Noonan et al., 2018, distributed under the terms of a Creative Commons Attribution (CC BY) license (https://creativecommons.org/licenses/by/4.0/).

Following successful detection of adhesion molecules *in vitro* and *ex vivo* (Noonan et al., 2018), we next designed an *in vivo* model for detecting expression of adhesion molecules in human vessels (Meehan et al., 2020). We engrafted human adipose tissue into immunocompromised NSG mice, which results in anastomosis between the human vessels and

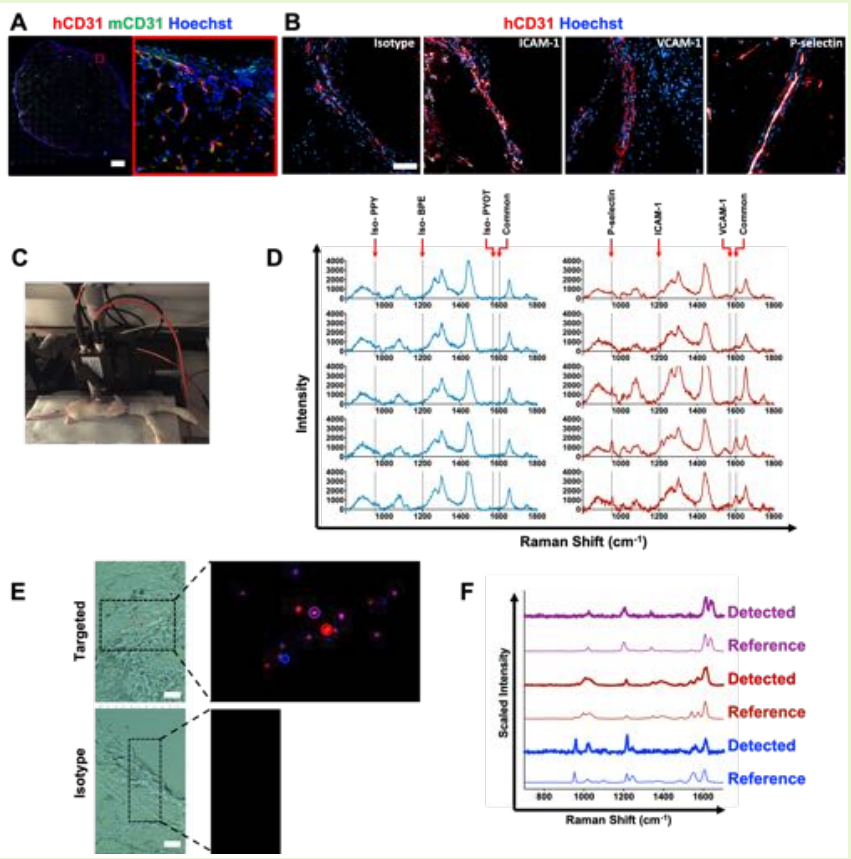

Figure 30. *In vivo* SERS-biofunctionalized NP molecular imaging of adhesion molecules. (**A**) Successful engraftment is shown by anastomosis of human and murine vessels at the periphery of the graft. Scale bar = 1000 µm. (**B**) Following human TNF-α treatment, ICAM-1 and P-selectin but not VCAM-1 are upregulated on the endothelium. Scale bar = 100 µm. (**C**) To perform in vivo SERS imaging, mice were anaesthetised, and SERS spectroscopy was performed on the graft site as shown in the experimental setup. (**D**) SERS spectra were acquired 24h later from mice injected with a mixture of human P-selectin, ICAM-1 and VCAM-1 targeted NPs (Red spectra) or respective isotype control NPs (Blue spectra). Peaks pertaining to the common region were present in all 5 animals and P-selectin, ICAM-1 and VCAM-1 showed increased signal intensity compared with isotype control treated mice indicating that NPs could successfully be detected bound to their target on human endothelium. Each spectrum is taken from a different animal. N = 5 mice per group. (**E**) Following *in vivo* spectroscopy, grafts were excised, and sections used for SERS microscopy. Tissue from mice that received the targeted NPs contained ICAM-1 NPs (purple), anti-VCAM-1 NPs (red) and anti–P-selectin NPs (blue). In isotype treated mice, no NPs were observed within the tissue sections. Scale bar = 20 µm. (**F**) The circles in the Raman map in (**E**) correlate with the acquired spectra shown in (**F**), shown alongside reference spectra for each Raman reporter. Reproduced from Noonan et al., 2018, distributed under the terms of a Creative Commons Attribution (CC BY) license (https://creativecommons.org/licenses/by/4.0/).

the mouse systemic vasculature within 3 weeks. Engrafted mice were then injected with human TNF-α to induce upregulation of endothelial adhesion molecules in the human graft vasculature. Subsequently, we injected a mixture of differentially functionalised SERS NPs and performed SERS spectroscopy and microscopy as described in Figure 30. In summary, the results from our study demonstrate the successful application of targeted SERS NP imaging *in vivo* for the non-invasive detection of endothelial adhesion molecules in a multiplexing manner (Noonan et al., 2018).

Figure 31 illustrates how SERS compares to our ideal molecular imaging tool from Figure 3. A comparison of Figures 28 and 31 further reveals that SERS has similar advantages to PAI, as well as some of the same limitations. However, SERS is a far less developed technology in terms of *in vivo* applications and is yet to be tested as an imaging tool on patients. SERS has exquisite sensitivity and spatial resolution, as well as fast acquisition times and high

multiplexing ability due to the narrow spectral bands of many Raman reporters (Figure 29). Like PAI, portable devices also exist, increasing the versatility and reducing cost of application. However, in contrast to PAI, SERS provides no anatomic information and external metallic based NPs are a prerequisite for generating the SERS signal, so this creates an additional barrier to in-human trials.

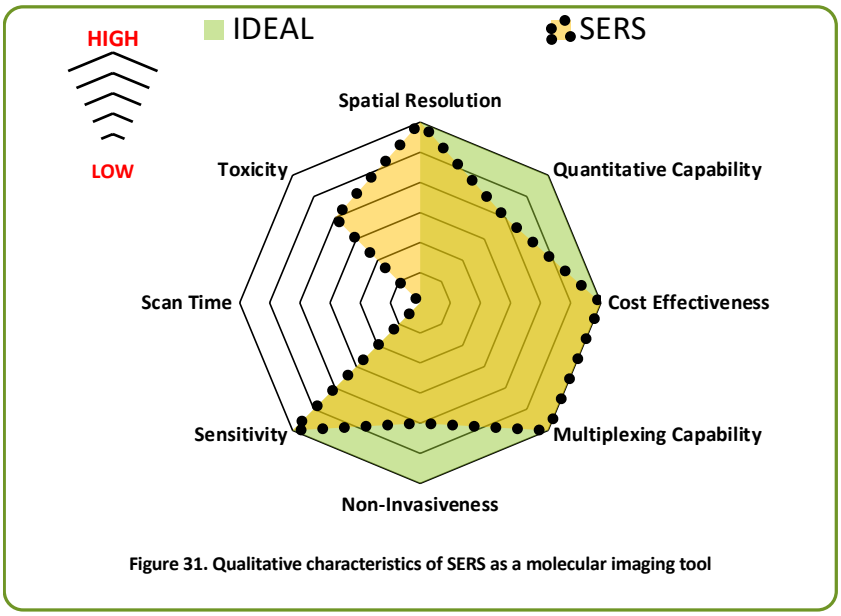

Figure 31. Qualitative characteristics of SERS as a molecular imaging tool

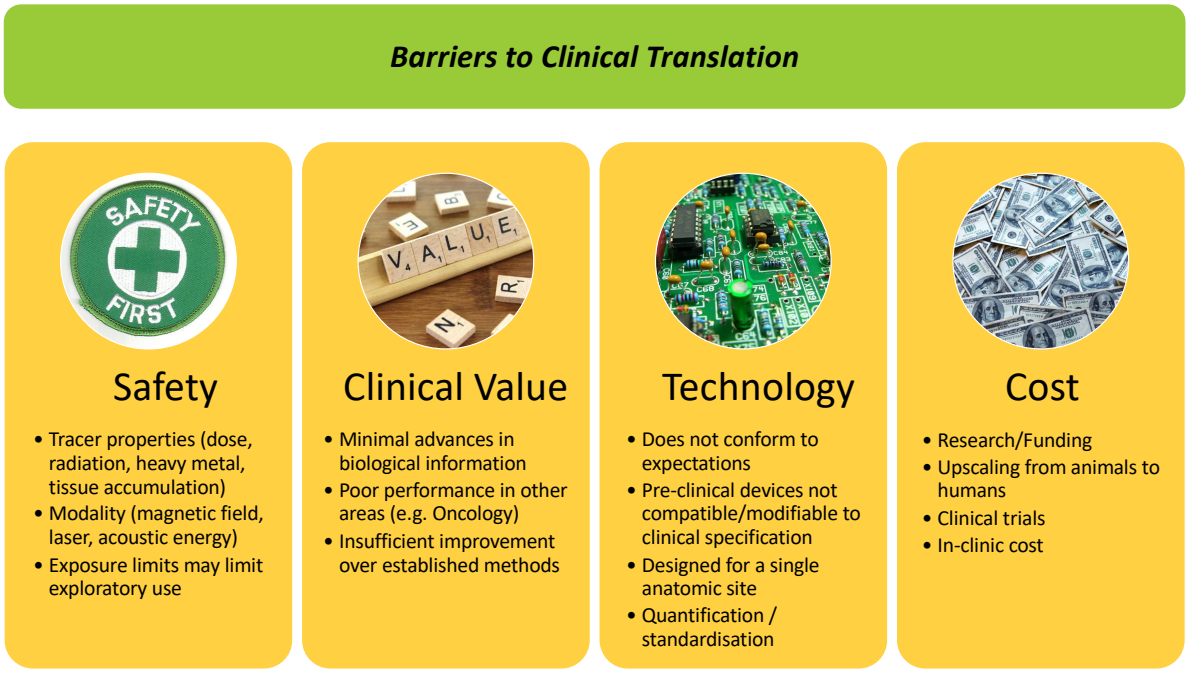

The major barriers that exist for clinical translation are categorized into four core areas, - cost, safety, technology and clinical value – that imaging technologies must address to satisfy regulatory and healthcare authorities. Examples are presented for each of these categories. Cost is a critical area, particularly with ever increasing pressures on healthcare funding. In the main,

imaging agents are less expensive to develop with respect to therapeutic compounds, but the converse is also true i.e. revenues are lower (Agdeppa and Spilker, 2009). With the timeline of development being similar, companies may choose to maximise revenue by diverting funds to therapeutics rather than imaging agents. Other costs include clinical-trial costs and implementation of new hardware and imaging agents. Costs can vary substantially with a PET unit costing many millions of pounds including the requirement of a cyclotron for synthesising PET radioligands. In contrast, the costs associated with clinical US scanning are considerably lower for both hardware, contrast agent production and post-analysis. Development costs also must be factored for upscaling research level technologies to those that meet the requirements and consistency of clinical level imaging i.e. the 'bench to bedside' transition.

Many candidate imaging molecules currently used in pre-clinical imaging carry too high a toxicity or are otherwise not suitable to clinical use. Therefore, designing tracers that minimise toxicity, while working in tandem with modalities that are proven safe for human use (e.g. safe laser and magnetic field strengths limits for optical and MRI based imaging respectively) will be essential. Since small molecule PET tracers are used in trace amounts, these compounds are generally clinically approved in a shorter time span due to reduced requirements for pre-clinical testing (Abou-Elkacem et al., 2015). Targeted microbubbles have also now been tested in human patients for the first time. Other than a few select metallic agents (most notably iron oxide-based particles for T2 MRI), small metallic based NPs have yet to reach clinical testing as imaging agents. However, there are a growing number of clinical trials, completed or ongoing that are testing gold-based NPs for photothermal ablation therapy in cancer, the most notable agent being the gold-based NP Aurolase® (Singh et al., 2018). Aurolase® is well tolerated and has similar physiochemical properties to the gold NPs used in pre-clinical PAI and SERS imaging. Furthermore, the use of gold-based NPs and photothermal therapy has shown promise in an early trial conducted on patients with coronary artery disease (Kharlamov et al., 2015). It would be hoped that as these compounds become established as safe for human use then regulatory bodies would look more favourably on these agents being tested for diagnostic imaging.

In addition to good biocompatibility/low toxicity, other desirable properties of imaging agents include high target specificity (either through high affinity small molecules or multi-valent NPs to minimise required dose and improve signal to noise), be readily manufactured and stable under storage, show favourable pharmacokinetics and ideally be adaptable to allow multi-modal imaging (Cicha et al., 2018; MacRitchie et al., 2020a). Versatility of use is also highly

desirable for a molecular imaging modality or tracer. Not only does this increase value for money but can improve clinical decision making due to integrated patient data. Examples of versatility may involve tracers that bind to molecules that are biomarkers of multiple diseases such as endothelial activation markers, thus allowing imaging of several CVDs or the use of equipment such as handheld devices that can image more than one anatomical site. Finally, devices that are multimodal, even involving modular type systems such as OCT-Raman or NIRF-Raman catheters may be used to derive molecular information of arterial disease. Ultimately, the implementation of a new technology or imaging agent will come down to whether it offers a significant improvement in diagnostic accuracy or monitoring of therapies over established methods. Incremental improvements will not be sufficient, particularly if the modality is novel or associated with high costs.

Closing Summary

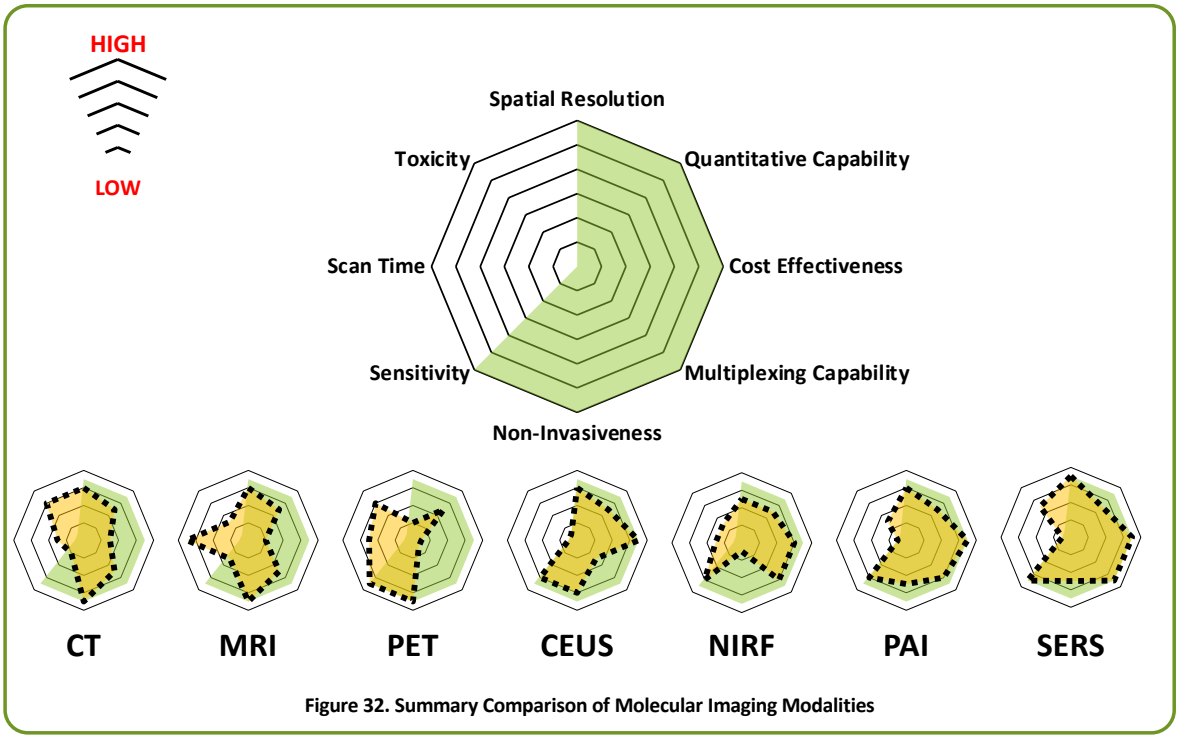

Figure 32. Summary Comparison of Molecular Imaging Modalities

Inflammation is key component of many CVDs and related metabolic conditions; therefore, it is essential that we can accurately determine how inflammation contributes to CVD risk and progression (Maffia et al., 2007; Fumagalli et al., 2011; Kennedy et al., 2013; Welsh et al., 2017; Cole et al., 2018; Sagan et al., 2019; MacRitchie et al., 2020b; Siedlinski et al, 2020; Nosalski et al., 2020). This requires understanding both the beneficial and detrimental inflammatory processes occurring within the patient and if inflammatory signatures can be used

to predict the course of a disease or response to therapy. The recent Canakinumab Anti-inflammatory Thrombosis Outcome Study (CANTOS) and Colchicine Cardiovascular Outcomes Trial (COLCOT) have shown that targeting inflammation in patients can reduce the risk of recurrent MACE (Ridker et al., 2017; Maffia & Guzik, 2019; Tardif et al., 2019). Yet C-reactive protein is a gross marker of inflammation and does not reveal the nature of the local inflammatory environment at the site of disease.

As an adjunct to imaging the human cardiovascular system, certain molecular imaging technologies such as SERS can be used for *in vitro* multiplexed assessment of blood biomarkers (molecular fingerprinting), with superior sensitivity to enzyme-linked immunosorbent assay (ELISA) (Kaminska et al., 2017). In addition to having the capacity to detect biomarkers at a lower concentration, techniques like SERS can screen many analytes in a blood sample at high speed, an advantage in the clinic since useful information from circulating inflammatory markers will likely require analysing the relative ratios of multiple cytokines and chemokines for disease profiling.

At present, imaging of CVD relies on assessment of the structural changes in the cardiovascular system, dependent on the underlying pathology. Such changes often present during advanced disease, thus limiting the opportunity for early detection. As described in this review, generalized inflammation can be detected within the vasculature and heart by current technologies such as MRI and PET but little information on the nature of the inflammation can be derived. Further analysis of inflammation is dependent on blood derived biomarkers and clinical scores. However, as already touched on, current serum biomarkers often show poor correlation with pathological processes. This limitation in our ability to quantify individual disease progression in inflammatory conditions impairs accurate diagnosis, therapeutic intervention and personalized medicine.

Molecular imaging has the potential to reveal deeper insights into cardiovascular inflammation and how it evolves over time. It may also be uniquely useful in situations in which clinical presentation is not accompanied by overt anatomical changes such as microvascular dysfunction (Ong et al., 2020). This review has provided a range of examples of how molecular imaging modalities - those already in clinical use and emerging technologies - can detect cardiovascular inflammation either directly or via the use of imaging agents. Multiple diagnostic imaging tools are already used in the diagnosis of CVD and this will likely continue in the future as molecular imaging evolves and is adopted as part of a multi-discipline diagnostic work up. For example, PET may be used with a tracer against a cytokine like IL-1β

or a chemokine receptor like CXCR4, alongside a low toxicity imaging device like CEUS or PAI, supplemented with biochemical and other cardiovascular measurements. The specific inflammatory targets deemed useful for clinical monitoring will likely themselves be partly determined by molecular imaging. In this regard, molecular imaging acts to both further disease's understanding by revealing disease-specific targets, and subsequently imaging those targets for diagnosis/monitoring. As we have also discussed, there is no perfect single molecular imaging modality, and some contain intrinsic limitations (poor spatial resolution and radiation exposure for PET) or have yet to be proven in clinical use (SERS). However, research is moving at pace with more sensitive forms of MRI being developed, significant increases in the number of PET trials testing novel ligands (including those that target inflammation) and the acceleration of PAI from research institutions to clinical trials.

Finally, advances in molecular imaging are happening in parallel with the availability of large data sets and the development of machine learning and artificial intelligence approaches, which have the power to revolutionise cardiovascular imaging, providing direct links between tissue biology and imaging phenotyping (Oikonomou et al., 2020). This will be crucial for better patient stratification and treatment. The chronic nature of many CVDs affords the opportunity for early detection, monitoring and prompt therapeutic action and in this regard, molecular imaging of inflammation has great potential to transform both the speed and accuracy of clinical decision making.

Acknowledgements

Our work was supported by the British Heart Foundation grants PG/12/81/29897, RE/13/5/30177 and PG/19/84/34771; the Engineering and Physical Sciences Research Council (EPSRC) grant EP/L014165/1; the Wellcome Trust grant 204820/Z/16/Z; and the University of Glasgow Scottish Funding Council and the Global Challenges Research Fund.

Conflict of Interest

The authors declare that the research was conducted in the absence of any commercial or financial relationships that could be construed as a potential conflict of interest.

References

Abou-Elkacem, L., Bachawal, S. V., & Willmann, J. K. (2015). Ultrasound molecular imaging: Moving toward clinical translation. *European Journal of Radiology, 84*(9), 1685-1693. doi:10.1016/j.ejrad.2015.03.016

Agdeppa, E. D., & Spilker, M. E. (2009). A review of imaging agent development. *The AAPS Journal*, *11*(2), 286–299. https://doi.org/10.1208/s12248-009-9104-5

Allen, T. J., Hall, A., Dhillon, A. P., Owen, J. S., & Beard, P. C. (2012). Spectroscopic photoacoustic imaging of lipid-rich plaques in the human aorta in the 740 to 1400 nm wavelength range. *Journal of Biomedical Optics*, *17*(6), 061209. https://doi.org/10.1117/1.JBO.17.6.061209

Antonopoulos, A. S., Sanna, F., Sabharwal, N., Thomas, S., Oikonomou, E. K., Herdman, L., Margaritis, M., Shirodaria, C., Kampoli, A. M., Akoumianakis, I., Petrou, M., Sayeed, R., Krasopoulos, G., Psarros, C., Ciccone, P., Brophy, C. M., Digby, J., Kelion, A., Uberoi, R., Anthony, S., … Antoniades, C. (2017). Detecting human coronary inflammation by imaging perivascular fat. *Science Translational Medicine*, *9*(398), eaal2658. https://doi.org/10.1126/scitranslmed.aal2658

Anzai, T. (2013). Post-infarction inflammation and left ventricular remodeling: a double-edged sword. *Circulation Journal, 77*(3), 580-587. doi:10.1253/circj.cj-13-0013

Brangsch, J., Reimann, C., Kaufmann, J. O., Adams, L. C., Onthank, D. C., Thöne-Reineke, C., Robinson, S. P., Buchholz, R., Karst, U., Botnar, R. M., Hamm, B., & Makowski, M. R. (2019). Concurrent Molecular Magnetic Resonance Imaging of Inflammatory Activity and Extracellular Matrix Degradation for the Prediction of Aneurysm Rupture. *Circulation. Cardiovascular Imaging*, *12*(3), e008707. https://doi.org/10.1161/CIRCIMAGING.118.008707

Bruns, O. T., Bischof, T. S., Harris, D. K., Franke, D., Shi, Y., Riedemann, L., Bartelt, A., Jaworski, F. B., Carr, J. A., Rowlands, C. J., Wilson, M., Chen, O., Wei, H., Hwang, G. W., Montana, D. M., Coropceanu, I., Achorn, O. B., Kloepper, J., Heeren, J., So, P., … Bawendi, M. G. (2017). Next-generation *in vivo* optical imaging with short-wave infrared quantum dots. *Nature Biomedical Engineering*, *1*, 0056. https://doi.org/10.1038/s41551-017-0056

Cicha, I., Chauvierre, C., Texier, I., Cabella, C., Metselaar, J. M., Szebeni, J., Dézsi, L., Alexiou, C., Rouzet, F., Storm, G., Stroes, E., Bruce, D., MacRitchie, N., Maffia, P., &

Letourneur, D. (2018). From design to the clinic: practical guidelines for translating cardiovascular nanomedicine. *Cardiovascular research*, *114*(13), 1714–1727. https://doi.org/10.1093/cvr/cvy219

Cole, J. E., Park, I., Ahern, D. J., Kassiteridi, C., Danso Abeam, D., Goddard, M. E., Green, P., Maffia, P., & Monaco, C. (2018). Immune cell census in murine atherosclerosis: cytometry by time of flight illuminates vascular myeloid cell diversity. *Cardiovascular Research*, *114*(10), 1360–1371. https://doi.org/10.1093/cvr/cvy109

Cormode, D. P., Roessl, E., Thran, A., Skajaa, T., Gordon, R. E., Schlomka, J. P., Fuster, V., Fisher, E. A., Mulder, W. J., Proksa, R., & Fayad, Z. A. (2010). Atherosclerotic plaque composition: analysis with multicolor CT and targeted gold nanoparticles. *Radiology*, *256*(3), 774–782. https://doi.org/10.1148/radiol.10092473

de la Zerda, A., Bodapati, S., Teed, R., May, S. Y., Tabakman, S. M., Liu, Z., Khuri-Yakub, B. T., Chen, X., Dai, H., & Gambhir, S. S. (2012). Family of enhanced photoacoustic imaging agents for high-sensitivity and multiplexing studies in living mice. *ACS Nano*, *6*(6), 4694–4701. https://doi.org/10.1021/nn204352r

Doughan, A. R., & Williams, B. R. (2006). Cardiac sarcoidosis. *Heart, 92*(2), 282-288. doi:10.1136/hrt.2005.080481

DSouza, A. V., Lin, H., Henderson, E. R., Samkoe, K. S., & Pogue, B. W. (2016). Review of fluorescence guided surgery systems: identification of key performance capabilities beyond indocyanine green imaging. *Journal of Biomedical Optics*, *21*(8), 80901. https://doi.org/10.1117/1.JBO.21.8.080901

Fumagalli, S., Coles, J. A., Ejlerskov, P., Ortolano, F., Bushell, T. J., Brewer, J. M., De Simoni, M. G., Dever, G., Garside, P., Maffia, P., & Carswell, H. V. (2011). In vivo real-time multiphoton imaging of T lymphocytes in the mouse brain after experimental stroke. *Stroke*, *42*(5), 1429–1436. https://doi.org/10.1161/STROKEAHA.110.603704

Gao, W., Li, X., Liu, Z., Fu, W., Sun, Y., Cao, W., Tong, L., & Tang, B. (2019). A Redox-Responsive Self-Assembled Nanoprobe for Photoacoustic Inflammation Imaging to Assess Atherosclerotic Plaque Vulnerability. *Analytical chemistry*, *91*(1), 1150–1156. https://doi.org/10.1021/acs.analchem.8b04912

Gulyás, B., Tóth, M., Schain, M., Airaksinen, A., Vas, A., Kostulas, K., Lindström, P., Hillert, J., & Halldin, C. (2012). Evolution of microglial activation in ischaemic core and peri-infarct

regions after stroke: a PET study with the TSPO molecular imaging biomarker [((11))C]vinpocetine. *Journal of the Neurological Sciences*, *320*(1-2), 110–117. https://doi.org/10.1016/j.jns.2012.06.026

Hong, G., Robinson, J. T., Zhang, Y., Diao, S., Antaris, A. L., Wang, Q., & Dai, H. (2012). In vivo fluorescence imaging with Ag2S quantum dots in the second near-infrared region. *Angewandte Chemie (International ed. in English)*, *51*(39), 9818–9821. https://doi.org/10.1002/anie.201206059

Htun, N. M., Chen, Y. C., Lim, B., Schiller, T., Maghzal, G. J., Huang, A. L., Elgass, K. D., Rivera, J., Schneider, H. G., Wood, B. R., Stocker, R., & Peter, K. (2017). Near-infrared autofluorescence induced by intraplaque hemorrhage and heme degradation as marker for high-risk atherosclerotic plaques. *Nature Communications*, *8*(1), 75. https://doi.org/10.1038/s41467-017-00138-x

Hulten, E., Aslam, S., Osborne, M., Abbasi, S., Bittencourt, M. S., & Blankstein, R. (2016). Cardiac sarcoidosis-state of the art review. *Cardiovascular Diagnosis and Therapy*, *6*(1), 50–63. https://doi.org/10.3978/j.issn.2223-3652.2015.12.13

Hyafil, F., Pelisek, J., Laitinen, I., Schottelius, M., Mohring, M., Döring, Y., van der Vorst, E. P., Kallmayer, M., Steiger, K., Poschenrieder, A., Notni, J., Fischer, J., Baumgartner, C., Rischpler, C., Nekolla, S. G., Weber, C., Eckstein, H. H., Wester, H. J., & Schwaiger, M. (2017). Imaging the Cytokine Receptor CXCR4 in Atherosclerotic Plaques with the Radiotracer ^{68}Ga-Pentixafor for PET. *The Journal of Nuclear Medicine*, *58*(3), 499–506. https://doi.org/10.2967/jnumed.116.179663

Ivankovic, I., Mercep, E., Schmedt, C. G., Dean-Ben, X. L., & Razansky, D. (2019). Real-time Volumetric Assessment of the Human Carotid Artery: Handheld Multispectral Optoacoustic Tomography. *Radiology, 291*(1), 45-50. doi:10.1148/radiol.2019181325

Jo, J., Xu, G., Cao, M., Marquardt, A., Francis, S., Gandikota, G., & Wang, X. (2017). A Functional Study of Human Inflammatory Arthritis Using Photoacoustic Imaging. *Scientific Reports, 7*(1), 15026. doi:10.1038/s41598-017-15147-5

Kahramangil, B., & Berber, E. (2017). The use of near-infrared fluorescence imaging in endocrine surgical procedures. *Journal of Surgical Oncology, 115*(7), 848-855. doi:10.1002/jso.24583

Kaminska, A., Winkler, K., Kowalska, A., Witkowska, E., Szymborski, T., Janeczek, A., & Waluk, J. (2017). SERS-based Immunoassay in a Microfluidic System for the Multiplexed Recognition of Interleukins from Blood Plasma: Towards Picogram Detection. *Scientific Reports, 7*(1), 10656. doi:10.1038/s41598-017-11152-w

Kaufmann, B. A., Carr, C. L., Belcik, J. T., Xie, A., Yue, Q., Chadderdon, S., Caplan, E. S., Khangura, J., Bullens, S., Bunting, S., & Lindner, J. R. (2010). Molecular imaging of the initial inflammatory response in atherosclerosis: implications for early detection of disease. *Arteriosclerosis, Thrombosis, and Vascular Biology*, *30*(1), 54–59. https://doi.org/10.1161/ATVBAHA.109.196386

Kennedy, S., Wu, J., Wadsworth, R. M., Lawrence, C. E., & Maffia, P. (2013). Mast cells and vascular diseases. *Pharmacology & Therapeutics*, *138*(1), 53–65. https://doi.org/10.1016/j.pharmthera.2013.01.001

Kharlamov, A. N., Tyurnina, A. E., Veselova, V. S., Kovtun, O. P., Shur, V. Y., & Gabinsky, J. L. (2015). Silica-gold nanoparticles for atheroprotective management of plaques: results of the NANOM-FIM trial. *Nanoscale, 7*(17), 8003-8015. doi:10.1039/c5nr01050k

Kolossváry, M., De Cecco, C. N., Feuchtner, G., & Maurovich-Horvat, P. (2019). Advanced atherosclerosis imaging by CT: Radiomics, machine learning and deep learning. *Journal of Cardiovascular Computed Tomography*, *13*(5), 274–280. https://doi.org/10.1016/j.jcct.2019.04.007

Kolossváry, M., Karády, J., Szilveszter, B., Kitslaar, P., Hoffmann, U., Merkely, B., & Maurovich-Horvat, P. (2017). Radiomic Features Are Superior to Conventional Quantitative Computed Tomographic Metrics to Identify Coronary Plaques With Napkin-Ring Sign. *Circulation. Cardiovascular Imaging*, *10*(12), e006843. https://doi.org/10.1161/CIRCIMAGING.117.006843

Kruizinga, P., van der Steen, A. F., de Jong, N., Springeling, G., Robertus, J. L., van der Lugt, A., & van Soest, G. (2014). Photoacoustic imaging of carotid artery atherosclerosis. *Journal of Biomedical Optics*, *19*(11), 110504. https://doi.org/10.1117/1.JBO.19.11.110504

Laing, S., Jamieson, L. E., Faulds, K., & Graham, D. (2017). Surface-enhanced Raman spectroscopy for in vivo biosensing. *Nature Reviews Chemistry, 1*(8), 0060. doi:10.1038/s41570-017-0060

Lamare, F., Hinz, R., Gaemperli, O., Pugliese, F., Mason, J. C., Spinks, T., Camici, P. G., & Rimoldi, O. E. (2011). Detection and quantification of large-vessel inflammation with 11C-(R)-PK11195 PET/CT. *Journal of Nuclear Medicine*, *52*(1), 33–39. https://doi.org/10.2967/jnumed.110.079038

Li, X., Heber, D., Leike, T., Beitzke, D., Lu, X., Zhang, X., Wei, Y., Mitterhauser, M., Wadsak, W., Kropf, S., Wester, H. J., Loewe, C., Hacker, M., & Haug, A. R. (2018). [68Ga]Pentixafor-PET/MRI for the detection of Chemokine receptor 4 expression in atherosclerotic plaques. *European Journal of Nuclear Medicine and Molecular Imaging*, *45*(4), 558–566. https://doi.org/10.1007/s00259-017-3831-0

Lim, B., Yao, Y., Huang, A. L., Yap, M. L., Flierl, U., Palasubramaniam, J., Zaldivia, M., Wang, X., & Peter, K. (2017). A Unique Recombinant Fluoroprobe Targeting Activated Platelets Allows *In Vivo* Detection of Arterial Thrombosis and Pulmonary Embolism Using a Novel Three-Dimensional Fluorescence Emission Computed Tomography (FLECT) Technology. *Theranostics*, *7*(5), 1047–1061. https://doi.org/10.7150/thno.18099

MacAskill, M. G., Newby, D. E., & Tavares, A. (2019). Frontiers in positron emission tomography imaging of the vulnerable atherosclerotic plaque. *Cardiovascular Research*, *115*(14), 1952–1962. https://doi.org/10.1093/cvr/cvz162

MacRitchie, N., Frleta-Gilchrist, M., Sugiyama, A., Lawton, T., McInnes, I. B., & Maffia, P. (2020a). Molecular imaging of inflammation - Current and emerging technologies for diagnosis and treatment. *Pharmacology & Therapeutics*, *211*, 107550. https://doi.org/10.1016/j.pharmthera.2020.107550

MacRitchie, N., Grassia, G., Noonan, J., Cole, J. E., Hughes, C. E., Schroeder, J., Benson, R. A., Cochain, C., Zernecke, A., Guzik, T. J., Garside, P., Monaco, C., & Maffia, P. (2020b). The aorta can act as a site of naïve CD4+ T-cell priming. *Cardiovascular Research*, *116*(2), 306–316. https://doi.org/10.1093/cvr/cvz102

MacRitchie, N., Grassia, G., Noonan, J., Garside, P., Graham, D., & Maffia, P. (2018). Molecular imaging of atherosclerosis: spotlight on Raman spectroscopy and surface-enhanced Raman scattering. *Heart, 104*(6), 460-467. doi:10.1136/heartjnl-2017-311447

Maffia, P., & Guzik, T. J. (2019) When, where, and how to target vascular inflammation in the post-CANTOS era?. *European Heart Journal, 40*(30), 2492-2494. doi:10.1093/eurheartj/ehz133

Maffia, P., Zinselmeyer, B. H., Ialenti, A., Kennedy, S., Baker, A. H., McInnes, I. B., Brewer, J. M., & Garside, P. (2007). Images in cardiovascular medicine. Multiphoton microscopy for 3-dimensional imaging of lymphocyte recruitment into apolipoprotein-E-deficient mouse carotid artery. *Circulation*, *115*(11), e326–e328. https://doi.org/10.1161/CIRCULATIONAHA.106.658492

Majmudar, M. D., & Nahrendorf, M. (2012). Cardiovascular molecular imaging: the road ahead. *The Journal of Nuclear Medicine*, *53*(5), 673–676. https://doi.org/10.2967/jnumed.111.099838

Marnane, M., Merwick, A., Sheehan, O. C., Hannon, N., Foran, P., Grant, T., Dolan, E., Moroney, J., Murphy, S., O'Rourke, K., O'Malley, K., O'Donohoe, M., McDonnell, C., Noone, I., Barry, M., Crowe, M., Kavanagh, E., O'Connell, M., & Kelly, P. J. (2012). Carotid plaque inflammation on 18F-fluorodeoxyglucose positron emission tomography predicts early stroke recurrence. *Annals of Neurology*, *71*(5), 709–718. https://doi.org/10.1002/ana.23553

McQueenie, R., Stevenson, R., Benson, R., MacRitchie, N., McInnes, I., Maffia, P., Faulds, K., Graham, D., Brewer, J., & Garside, P. (2012). Detection of inflammation in vivo by surface-enhanced Raman scattering provides higher sensitivity than conventional fluorescence imaging. *Analytical Chemistry*, *84*(14), 5968–5975. https://doi.org/10.1021/ac3006445

Meehan, G. R., Scales, H. E., Osii, R., De Niz, M., Lawton, J. C., Marti, M., Garside, P., Craig, A., & Brewer, J. M. (2020). Developing a xenograft model of human vasculature in the mouse ear pinna. *Scientific Reports*, *10*(1), 2058. https://doi.org/10.1038/s41598-020-58650-y

Mulder, W. J., Jaffer, F. A., Fayad, Z. A., & Nahrendorf, M. (2014). Imaging and nanomedicine in inflammatory atherosclerosis. *Science Translational Medicine*, *6*(239), 239sr1. https://doi.org/10.1126/scitranslmed.3005101

Nazir, M. S., & Nicol, E. (2019). The SCOT-HEART trial: cardiac CT to guide patient management and improve outcomes. *Cardiovascular Research*, *115*(10), e88–e90. https://doi.org/10.1093/cvr/cvz173

Nosalski, R., & Guzik, T. J. (2017). Perivascular adipose tissue inflammation in vascular disease. *British Journal of Pharmacology*, *174*(20), 3496–3513. https://doi.org/10.1111/bph.13705

Nosalski, R., Siedlinski, M., Denby, L., McGinnigle, E., Nowak, M., Cat, A., Medina-Ruiz, L., Cantini, M., Skiba, D., Wilk, G., Osmenda, G., Rodor, J., Salmeron-Sanchez, M., Graham, G.,

Maffia, P., Graham, D., Baker, A. H., & Guzik, T. J. (2020). T-Cell-Derived miRNA-214 Mediates Perivascular Fibrosis in Hypertension. *Circulation Research*, *126*(8), 988–1003. https://doi.org/10.1161/CIRCRESAHA.119.315428

Noonan, J., Asiala, S. M., Grassia, G., MacRitchie, N., Gracie, K., Carson, J., Moores, M., Girolami, M., Bradshaw, A. C., Guzik, T. J., Meehan, G. R., Scales, H. E., Brewer, J. M., McInnes, I. B., Sattar, N., Faulds, K., Garside, P., Graham, D., & Maffia, P. (2018). *In vivo* multiplex molecular imaging of vascular inflammation using surface-enhanced Raman spectroscopy. *Theranostics*, *8*(22), 6195–6209. https://doi.org/10.7150/thno.28665

Oikonomou, E. K., Marwan, M., Desai, M. Y., Mancio, J., Alashi, A., Hutt Centeno, E., Thomas, S., Herdman, L., Kotanidis, C. P., Thomas, K. E., Griffin, B. P., Flamm, S. D., Antonopoulos, A. S., Shirodaria, C., Sabharwal, N., Deanfield, J., Neubauer, S., Hopewell, J. C., Channon, K. M., Achenbach, S., … Antoniades, C. (2018). Non-invasive detection of coronary inflammation using computed tomography and prediction of residual cardiovascular risk (the CRISP CT study): a post-hoc analysis of prospective outcome data. *Lancet (London, England)*, *392*(10151), 929–939. https://doi.org/10.1016/S0140-6736(18)31114-0

Oikonomou, E. K., Siddique, M., & Antoniades, C. (2020). Artificial intelligence in medical imaging: A radiomic guide to precision phenotyping of cardiovascular disease. *Cardiovascular Research*, cvaa021. Advance online publication. https://doi.org/10.1093/cvr/cvaa021

Oikonomou, E. K., Williams, M. C., Kotanidis, C. P., Desai, M. Y., Marwan, M., Antonopoulos, A. S., Thomas, K. E., Thomas, S., Akoumianakis, I., Fan, L. M., Kesavan, S., Herdman, L., Alashi, A., Centeno, E. H., Lyasheva, M., Griffin, B. P., Flamm, S. D., Shirodaria, C., Sabharwal, N., Kelion, A., … Antoniades, C. (2019). A novel machine learning-derived radiotranscriptomic signature of perivascular fat improves cardiac risk prediction using coronary CT angiography. *European Heart Journal*, *40*(43), 3529–3543. https://doi.org/10.1093/eurheartj/ehz592

Ong, P., Safdar, B., Seitz, A., Hubert, A., Beltrame, J. F., & Prescott, E. (2020). Diagnosis of coronary microvascular dysfunction in the clinic. *Cardiovascular Research*, *116*(4), 841–855. https://doi.org/10.1093/cvr/cvz339

Osborne, M. T., Hulten, E. A., Singh, A., Waller, A. H., Bittencourt, M. S., Stewart, G. C., Hainer, J., Murthy, V. L., Skali, H., Dorbala, S., Di Carli, M. F., & Blankstein, R. (2014). Reduction in ^{18}F-fluorodeoxyglucose uptake on serial cardiac positron emission tomography is

associated with improved left ventricular ejection fraction in patients with cardiac sarcoidosis. *Journal of Nuclear Cardiology*, *21*(1), 166–174. https://doi.org/10.1007/s12350-013-9828-6

Otsuka, K., Fukuda, S., Tanaka, A., Nakanishi, K., Taguchi, H., Yoshikawa, J., Shimada, K., & Yoshiyama, M. (2013). Napkin-ring sign on coronary CT angiography for the prediction of acute coronary syndrome. *JACC. Cardiovascular Imaging*, *6*(4), 448–457. https://doi.org/10.1016/j.jcmg.2012.09.016

Pedersen, S. F., Sandholt, B. V., Keller, S. H., Hansen, A. E., Clemmensen, A. E., Sillesen, H., Højgaard, L., Ripa, R. S., & Kjær, A. (2015). 64Cu-DOTATATE PET/MRI for Detection of Activated Macrophages in Carotid Atherosclerotic Plaques: Studies in Patients Undergoing Endarterectomy. *Arteriosclerosis, Thrombosis, and Vascular Biology*, *35*(7), 1696–1703. https://doi.org/10.1161/ATVBAHA.114.305067

Ramos, I. T., Henningsson, M., Nezafat, M., Lavin, B., Lorrio, S., Gebhardt, P., Protti, A., Eykyn, T. R., Andia, M. E., Flögel, U., Phinikaridou, A., Shah, A. M., & Botnar, R. M. (2018). Simultaneous Assessment of Cardiac Inflammation and Extracellular Matrix Remodeling after Myocardial Infarction. *Circulation. Cardiovascular Imaging*, *11*(11), e007453. https://doi.org/10.1161/CIRCIMAGING.117.007453

Ridker, P. M., Everett, B. M., Thuren, T., MacFadyen, J. G., Chang, W. H., Ballantyne, C., Fonseca, F., Nicolau, J., Koenig, W., Anker, S. D., Kastelein, J., Cornel, J. H., Pais, P., Pella, D., Genest, J., Cifkova, R., Lorenzatti, A., Forster, T., Kobalava, Z., Vida-Simiti, L., … CANTOS Trial Group (2017). Antiinflammatory Therapy with Canakinumab for Atherosclerotic Disease. *The New England Journal of Medicine*, *377*(12), 1119–1131. https://doi.org/10.1056/NEJMoa1707914

Ruiz-Cabello, J., Barnett, B. P., Bottomley, P. A., & Bulte, J. W. (2011). Fluorine (19F) MRS and MRI in biomedicine. *NMR in Biomedicine, 24*(2), 114-129. doi:10.1002/nbm.1570

Sagan, A., Mikolajczyk, T. P., Mrowiecki, W., MacRitchie, N., Daly, K., Meldrum, A., Migliarino, S., Delles, C., Urbanski, K., Filip, G., Kapelak, B., Maffia, P., Touyz, R., & Guzik, T. J. (2019). T Cells Are Dominant Population in Human Abdominal Aortic Aneurysms and Their Infiltration in the Perivascular Tissue Correlates With Disease Severity. *Frontiers in Immunology*, *10*, 1979. https://doi.org/10.3389/fimmu.2019.01979

Scales, H. E., Ierna, M., Smith, K. M., Ross, K., Meiklejohn, G. R., Patterson-Kane, J. C., McInnes, I. B., Brewer, J. M., Garside, P., & Maffia, P. (2016). Assessment of murine collagen-induced arthritis by longitudinal non-invasive duplexed molecular optical imaging.

Rheumatology (Oxford, England), *55*(3), 564–572. https://doi.org/10.1093/rheumatology/kev361

Schinkel, A. F., Kaspar, M., & Staub, D. (2016). Contrast-enhanced ultrasound: clinical applications in patients with atherosclerosis. *The International Journal of Cardiovascular Imaging*, *32*(1), 35–48. https://doi.org/10.1007/s10554-015-0713-z

Schneider, M., Anantharam, B., Arditi, M., Bokor, D., Broillet, A., Bussat, P., Fouillet, X., Frinking, P., Tardy, I., Terrettaz, J., Senior, R., & Tranquart, F. (2011). BR38, a new ultrasound blood pool agent. *Investigative Radiology*, *46*(8), 486–494. https://doi.org/10.1097/RLI.0b013e318217b821

Siedlinski, M., Jozefczuk, E., Xu, X., Teumer, A., Evangelou, E., Schnabel, R. B., Welsh, P., Maffia, P., Erdmann, J., Tomaszewski, M., Caulfield, M. J., Sattar, N., Holmes, M. V., & Guzik, T. J. (2020). White Blood Cells and Blood Pressure: A Mendelian Randomization Study. *Circulation*, *141*(16), 1307–1317. https://doi.org/10.1161/CIRCULATIONAHA.119.045102

Singh, P., Pandit, S., Mokkapati, V., Garg, A., Ravikumar, V., & Mijakovic, I. (2018). Gold Nanoparticles in Diagnostics and Therapeutics for Human Cancer. *The International Journal of Molecular Sciences, 19*(7). doi:10.3390/ijms19071979

Sinharay, S., & Pagel, M. D. (2016). Advances in Magnetic Resonance Imaging Contrast Agents for Biomarker Detection. *Annual Review of Analytical Chemistry (Palo Alto, Calif.)*, *9*(1), 95–115. https://doi.org/10.1146/annurev-anchem-071015-041514

Steinberg, I., Huland, D. M., Vermesh, O., Frostig, H. E., Tummers, W. S., & Gambhir, S. S. (2019). Photoacoustic clinical imaging. *Photoacoustics, 14*, 77-98. doi:10.1016/j.pacs.2019.05.001

Steinl, D. C., Xu, L., Khanicheh, E., Ellertsdottir, E., Ochoa-Espinosa, A., Mitterhuber, M., Glatz, K., Kuster, G. M., & Kaufmann, B. A. (2016). Noninvasive Contrast-Enhanced Ultrasound Molecular Imaging Detects Myocardial Inflammatory Response in Autoimmune Myocarditis. *Circulation. Cardiovascular imaging*, *9*(8), e004720. https://doi.org/10.1161/CIRCIMAGING.116.004720

Tardif, J. C., Kouz, S., Waters, D. D., Bertrand, O. F., Diaz, R., Maggioni, A. P., Pinto, F. J., Ibrahim, R., Gamra, H., Kiwan, G. S., Berry, C., López-Sendón, J., Ostadal, P., Koenig, W., Angoulvant, D., Grégoire, J. C., Lavoie, M. A., Dubé, M. P., Rhainds, D., Provencher, M., …

Roubille, F. (2019). Efficacy and Safety of Low-Dose Colchicine after Myocardial Infarction. *The New England Journal of Medicine*, *381*(26), 2497–2505. https://doi.org/10.1056/NEJMoa1912388

Tarkin, J. M., Joshi, F. R., Evans, N. R., Chowdhury, M. M., Figg, N. L., Shah, A. V., Starks, L. T., Martin-Garrido, A., Manavaki, R., Yu, E., Kuc, R. E., Grassi, L., Kreuzhuber, R., Kostadima, M. A., Frontini, M., Kirkpatrick, P. J., Coughlin, P. A., Gopalan, D., Fryer, T. D., Buscombe, J. R., … Rudd, J. H. (2017). Detection of Atherosclerotic Inflammation by ^{68}Ga-DOTATATE PET Compared to [^{18}F]FDG PET Imaging. *Journal of the American College of Cardiology*, *69*(14), 1774–1791. https://doi.org/10.1016/j.jacc.2017.01.060

Ughi, G. J., Wang, H., Gerbaud, E., Gardecki, J. A., Fard, A. M., Hamidi, E., Vacas-Jacques, P., Rosenberg, M., Jaffer, F. A., & Tearney, G. J. (2016). Clinical Characterization of Coronary Atherosclerosis With Dual-Modality OCT and Near-Infrared Autofluorescence Imaging. *JACC. Cardiovascular Imaging*, *9*(11), 1304–1314. https://doi.org/10.1016/j.jcmg.2015.11.020

Valluru, K. S., Wilson, K. E., & Willmann, J. K. (2016). Photoacoustic Imaging in Oncology: Translational Preclinical and Early Clinical Experience. *Radiology, 280*(2), 332-349. doi:10.1148/radiol.16151414

Van Linthout, S., & Tschöpe, C. (2018). Viral myocarditis: a prime example for endomyocardial biopsy-guided diagnosis and therapy. *Current Opinion in Cardiology*, *33*(3), 325–333. https://doi.org/10.1097/HCO.0000000000000515

Verjans, J. W., Osborn, E. A., Ughi, G. J., Calfon Press, M. A., Hamidi, E., Antoniadis, A. P., Papafaklis, M. I., Conrad, M. F., Libby, P., Stone, P. H., Cambria, R. P., Tearney, G. J., & Jaffer, F. A. (2016). Targeted Near-Infrared Fluorescence Imaging of Atherosclerosis: Clinical and Intracoronary Evaluation of Indocyanine Green. *JACC. Cardiovascular imaging*, *9*(9), 1087–1095. https://doi.org/10.1016/j.jcmg.2016.01.034

Wang, X., Hagemeyer, C. E., Hohmann, J. D., Leitner, E., Armstrong, P. C., Jia, F., Olschewski, M., Needles, A., Peter, K., & Ahrens, I. (2012). Novel single-chain antibody-targeted microbubbles for molecular ultrasound imaging of thrombosis: validation of a unique noninvasive method for rapid and sensitive detection of thrombi and monitoring of success or failure of thrombolysis in mice. *Circulation*, *125*(25), 3117–3126. https://doi.org/10.1161/CIRCULATIONAHA.111.030312

Weiberg, D., Thackeray, J. T., Daum, G., Sohns, J. M., Kropf, S., Wester, H. J., Ross, T. L., Bengel, F. M., & Derlin, T. (2018). Clinical Molecular Imaging of Chemokine Receptor CXCR4 Expression in Atherosclerotic Plaque Using ^{68}Ga-Pentixafor PET: Correlation with Cardiovascular Risk Factors and Calcified Plaque Burden. *Journal of Nuclear Medicine*, *59*(2), 266–272. https://doi.org/10.2967/jnumed.117.196485

Welsh, P., Grassia, G., Botha, S., Sattar, N., & Maffia, P. (2017). Targeting inflammation to reduce cardiovascular disease risk: a realistic clinical prospect?. *British Journal of Pharmacology*, *174*(22), 3898–3913. https://doi.org/10.1111/bph.13818

Willmann, J. K., Bonomo, L., Testa, A. C., Rinaldi, P., Rindi, G., Valluru, K. S., Petrone, G., Martini, M., Lutz, A. M., & Gambhir, S. S. (2017). Ultrasound Molecular Imaging With BR55 in Patients With Breast and Ovarian Lesions: First-in-Human Results. *Journal of Clinical Oncology*, *35*(19), 2133–2140. https://doi.org/10.1200/JCO.2016.70.8594

Willmann, J. K., Cheng, Z., Davis, C., Lutz, A. M., Schipper, M. L., Nielsen, C. H., & Gambhir, S. S. (2008). Targeted microbubbles for imaging tumor angiogenesis: assessment of whole-body biodistribution with dynamic micro-PET in mice. *Radiology, 249*(1), 212-219. doi:10.1148/radiol.2491072050

Woodside, D. G., Tanifum, E. A., Ghaghada, K. B., Biediger, R. J., Caivano, A. R., Starosolski, Z. A., Khounlo, S., Bhayana, S., Abbasi, S., Craft, J. W., Jr, Maxwell, D. S., Patel, C., Stupin, I. V., Bakthavatsalam, D., Market, R. V., Willerson, J. T., Dixon, R., Vanderslice, P., & Annapragada, A. V. (2018). Magnetic Resonance Imaging of Atherosclerotic Plaque at Clinically Relevant Field Strengths (1T) by Targeting the Integrin α4β1. *Scientific Reports*, *8*(1), 3733. https://doi.org/10.1038/s41598-018-21893-x

Wu, C., Li, F., Niu, G., & Chen, X. (2013). PET imaging of inflammation biomarkers. *Theranostics, 3*(7), 448-466. doi:10.7150/thno.6592

Wüst, R., Calcagno, C., Daal, M., Nederveen, A. J., Coolen, B. F., & Strijkers, G. J. (2019). Emerging Magnetic Resonance Imaging Techniques for Atherosclerosis Imaging. *Arteriosclerosis, Thrombosis, and Vascular Biology*, *39*(5), 841–849. https://doi.org/10.1161/ATVBAHA.118.311756

Zainon, R., Ronaldson, J. P., Janmale, T., Scott, N. J., Buckenham, T. M., Butler, A. P., Butler, P. H., Doesburg, R. M., Gieseg, S. P., Roake, J. A., & Anderson, N. G. (2012). Spectral CT of carotid atherosclerotic plaque: comparison with histology. *European Radiology*, *22*(12), 2581–2588. https://doi.org/10.1007/s00330-012-2538-7

Zhang, H. F., Maslov, K., Stoica, G., & Wang, L. V. (2006). Functional photoacoustic microscopy for high-resolution and noninvasive in vivo imaging. *Nature Biotechnology, 24*(7), 848-851. doi:10.1038/nbt1220